CONSTRUCTION OF A SQUID-BASED DC SUSCEPTIBILITY MEASUREMENT SYSTEM AND ITS USE IN OBSERVING THE SUPERCONDUCTING TRANSITION OF SMALL $TaS_2(ANILINE)_{3/4}$ CRYSTALS

by

FREDERICK WILMOT GUPTILL

B.Sc.Eng-Phys., Dalhousie University, 1974

A THESIS SUBMITTED IN PARTIAL FULFILLMENT

OF THE REQUIREMENTS FOR THE DEGREE OF

MASTER OF SCIENCE

in the Department

of

Physics

SIMON FRASER UNIVERSITY

June 1977

APPROVAL

Name: Frederick Wilmot Guptill

Degree: Master of Science

Title of Thesis: Construction of a SQUID-based DC Susceptibility Measurement System and its use in Observing the Superconducting Transition of Small $TaS_2(aniline)_{3/4}$ Crystals

Examining Committee:

Chairman: Dr. D.J. Huntley

Dr. S. Gygax
Senior Supervisor

Dr. B.P. Clayman

Dr. J.F. Cochran

Dr. R.F. Frindt
Associate Professor
Department of Physics

Date Approved: 22 June 77

PARTIAL COPYRIGHT LICENSE

I hereby grant to Simon Fraser University the right to lend my thesis or dissertation (the title of which is shown below) to users of the Simon Fraser University Library, and to make partial or single copies only for such users or in response to a request from the library of any other university, or other educational institution, on its own behalf or for one of its users. I further agree that permission for multiple copying of this thesis for scholarly purposes may be granted by me or the Dean of Graduate Studies. It is understood that copying or publication of this thesis for financial gain shall not be allowed without my written permission.

Title of Thesis/Dissertation:

Construction of a SQUID-based DC Susceptibility Measurement System and its use in observing the Superconducting Transition of small $TaS_2(aniline)_{3/4}$ crystals

Author:

(signature)

Frederick Wilmot Guptill

(name)

6 Jul 77

(date)

ABSTRACT

Intercalated layered compounds have been the subject of tremendous practical and theoretical interest in recent years. Observations of some workers indicate the possibility of size-dependent effects in very small samples of these materials.

This thesis deals with the construction of a sensitive magnetometer and its use in observing the magnetic transitions of small superconducting samples.

Performance of the apparatus is analyzed both theoretically and experimentally. Results of these analyses are shown to be in reasonable agreement.

Unexpected results are obtained in measurements performed upon samples of $TaS_2(aniline)_{3/4}$. Calculations of some of the superconducting parameters of $TaS_2(aniline)_{3/4}$ are made in an attempt to explain the observations.

To Melody

ACKNOWLEDGMENTS

I would like to thank the faculty and staff of the Simon Fraser Physics department for technical support and assistance, the National Research Council and Simon Fraser University for financial support, and friends and relatives for personal support.

TABLE OF CONTENTS

	Page
Abstract	iii
Dedication	iv
Acknowledgements	v
List of Tables	viii
List of Figures	ix
Introduction and Motivation	1
Cryostat Design	6
Introduction	6
Temperature Control	9
Heat Leaks	9
Thermal Anchor	10
Pumping Lines	12
Epoxy	13
Miscellaneous	16
SQUID	18
Introduction	18
Flux Transformer	22
Cryostat Construction Materials	23
Ambient Fields	24
Vibration	25
Electrical Noise	26
Temperature Stability	27
Field Coil	29
Thermometer	32
Sample Preparation	38

	Page
Sample Substrate	40
Data Processing	42
Thermometry	42
SQUID Signal (Theoretical)	49
SQUID Signal (Experimental)	56
Experimental Results and Conclusions	60
Flux Pinning	60
Transition Widths	64
Transition Amplitudes	65
Calculation A	66
Calculation B	70
Suggestions for Further Work	79
Appendices	
A - Feedthroughs	82
B - Liquid Nitrogen Controller	84
C - Epoxy Curing Recipe	88
D - Cryostat Operating Procedures	91
E - Apparatus Specifications	94
F - Mean Free Path of He^4 Gas	98
G - Pressure Drops in Tubing	99
H - Second Flux Transformer	100
Notes	104
References	105

LIST OF TABLES

Table		Page
I	Viscosity of He^4 Gas	13
II	Dimensions of Samples	38
III	Critical Temperatures and Field For Marker Samples	47
IV	Numerical Results - Experimental and Calculated	73

LIST OF FIGURES

Figure		Page
1	Schematic diagram of cryostat.	7
2	Lower portion of cryostat.	8
3	One of the two epoxy-to-metal vacuum seals used in the cryostat.	15
4	Two cross-sectional views through center of SQUID.	19
5	SQUID mounting assembly.	20
6	Typical RF-biased SQUID system.	21
7	Optimum RF level for operation of our SQUID.	28
8	Constant current power supply used in four-terminal arrangement for resistance thermometry.	33
9	Residuals of single-interval thermometer curve fit.	35
10	Residuals of the final 3-interval fit for one of the two thermometers used.	36
11	Schematic model for heat flow in Sample Chamber.	44
12	Typical raw data plots.	43
13	Schematic model for heat flow in Sample Chamber.	48
14	Model for coupling of sample to the two pickup loops.	51
15	SQUID signal calibration points.	58
16	Transitions of $TaS_2(aniline)_{3/4}$ samples of various sizes.	61
17	Superconducting transitions of $TaS_2(aniline)_{3/4}$ sample #19 in various fields.	62
18	Superconducting transition of tin.	63
19	Transition of $TaS_2(aniline)_{3/4}$ taken from Reference 16.	75
20	Observed transition temperatures of $TaS_2(aniline)_{3/4}$ samples with field applied parallel to the layers.	77
21	Liquid nitrogen level controller.	85
22	Mean free path of He^4 gas.	98

Figure		Page
23	Pressure drop per unit length in circular tubing carrying He^4 gas.	99
24	Second flux transformer schematic.	101

INTRODUCTION AND MOTIVATION

In recent years there has been considerable interest in superconducting materials that display one-dimensional (1-D) or two-dimensional (2-D) properties and studies of 1-D and 2-D superconductors have proceeded along several paths.

Experimentally, the first problem is to construct, in a 3-D world, a superconducting system which is not 3-D. In particular, one wants to restrict superconducting electrons to motion in a plane (2-D) or in a line (1-D). One approach to this problem consists of constructing thin films or whiskers of superconducting materials. Another technique is to search for materials which have an intrinsic structure such that electron motion is inherently restricted. Ultimately, of course, the samples with which one works must be 3-D, but if any dimension is shorter than the superconducting coherence length, then that dimension can be regarded as absent.

The quasi-2-D materials, which we will group under the heading of layer compounds, are mostly transition metal dichalcogenides (TX_2's). This is an exciting group of compounds which have been the subject of experimentation since the 1920's. The metallic (T) component is from one of Groups IVB, VB, or VIB of the Periodic Table. The chalcogen (X) is one of sulfur, selenium, or tellurium. The TX_2's form crystalline structures made up of stacked

sandwiches. Each sandwich consists of two layers of chalcogen atoms with a single layer of metal atoms between. Binding is strong within sandwiches but weak and Van der Waals between sandwiches. These sandwiches are stacked in an ordered fashion, so, by varying the stacking sequence, one can create several different polymorphs.

TX_2's have generated interest for several reasons:

Thompson et al (Reference 60) have observed a metal-insulator transition in 1T-TaS_2.

Some TX_2's are good materials for observation of charge density waves. (See Reference 74.)

A further cause for interest in TX_2's is the discovery (Reference 1) of relatively high temperature (~10K) superconductivity in a related compound, $Li_{.3}Ti_{1.1}S_2$. TX_2's cover the range of superconducting T_C's from .8K (for TaS_2) to 7K (for $NbSe_2$).

It has been discovered that many of these compounds can be intercalated with alkali metals (Reference 64) and organic molecules (References 23,24), dramatically increasing anisotropy. Due to their layered structure and high effective surface area, the intercalated TX_2's make both good lubricants and good absorbers. There are exciting prospects related to the utilization of these absorbent properties in charge storage, possibly supplanting traditional types of storage batteries.

Many of these compounds are superconducting both before and after intercalation, which makes them exciting new tools for the study of anisotropy and dimensionality effects. Since 1970, study in this field has led to the discovery of probably more than 100 new layered superconductors.

As might be expected, judging from their structure, intercalated layered compounds display marked anisotropy. In some cases their normal state resistivity varies by five orders of magnitude depending upon direction of conduction through the crystal. Extreme anisotropy in the superconducting critical fields has also been observed (References 20,48).

Reports (References 50,71) of positive curvature of H_{C2} (the upper critical field) as a function of T have also spurred interest in several of the layer compounds. Prober (Reference 50) has measured $H_{C2//}$'s (upper critical field parallel to the layers) exceeding 150 kG in $TaS_2(pyridine)_{1/2}$ (i.e. TaS_2 intercalated with pyridine), and critical field slopes as high as 200 kG/K in the $TaS_{1.6}Se_{.4}$ intercalated compounds. This same author has speculated on the possibility of using layered superconductors as detectors of electromagnetic radiation by utilizing the Josephson-type coupling between the layers.

Initially much work was concentrated upon studies of fluctuation phenomena above the superconducting transition temperature (T_C) in

hopes of finding fluctuation behaviour characteristic of a 2-D superconductor. However, the weight of theoretical (References 26,38,39) and experimental (References 25,50,51) work seems to indicate that the fluctuation behaviour observed to date is indicative not of a 2-D system but of a highly anisotropic 3-D system. Moreover, according to some workers (References 25,46), 2-D effects should be most apparent below T_C.

Experimental results seem to indicate the presence of a significant number of interlayer connections (Reference 59). These shorts might be crystalline imperfections in which some layers run perpendicular to the majority of layers in the sample, metallic impurities or excess metal atoms trapped between the layers, or perhaps screw dislocations which are formed during growth of the crystal. The existence of screw dislocations in these materials has been confirmed by optical microscopy. The proclivity for the layer disulfides to crystallize with excess metal is well documented (Reference 70).

Motivation for the present investigation was supplied primarily by I-V curves (S. Gygax, private communication) obtained by means of four-terminal measurements upon small crystallites. Results seemed to indicate a dramatic lowering of T_C for some very small samples. Since one could reasonably expect a decrease in the number of crystal

imperfections with decreasing crystallite size, these results could be an indication of intrinsic 2-D behaviour in intercalated layer compounds. However, due to the difficulties involved in attaching leads to such small samples, interpretation of resistivity measurements is most ambiguous. One would like to confirm these results by means of a susceptibility measurement, which does away with the need for affixing electrical contacts to the samples. Prober has reported (Reference 50) unexplained T_c shifts in $TaS_2(aniline)_{3/4}$ observed by such a technique.

TaS_2 is formed at an elevated temperature in the 1T phase. Upon cooling to room temperature, the material spontaneously transforms to its 2H polymorph. It is the accompanying change in the volume of the crystallographic unit cell which may be responsible for a large number of the interlayer shorts. Prober has suggested that samples of dimensions of a fraction of a millimeter, or less, ought to be relatively free of such defects.

The object of this present work is to perform magnetization measurements upon very small crystals of $TaS_2(aniline)_{3/4}$ with the assumption that the number of interlayer shorts will decrease (and hopefully vanish before the sample does) with decreasing sample size.

CRYOSTAT DESIGN

INTRODUCTION: Published results (Reference 16) indicate that the normal-superconducting transition of $TaS_2(aniline)_{3/4}$ takes place between 2K and 3K. A simple He^4 evaporation cryostat is the obvious choice for working in this temperature regime. Figure 1 is a schematic diagram of the cryostat and associated apparatus which was used in this investigation. Figure 2 shows the details of the "business end" of the system. The equipment is of fairly standard design apart from two important features:

1)The use of a SQUID magnetometer system makes possible the measurement of very small changes in the DC susceptibility of a sample. A Meissner Effect was readily observable in tin samples of volume .007 mm^3.

2)Samples can be changed while in operation without having to warm the whole cryostat to room temperature.

The following description of the design and evolution of this cryostat is not intended to be complete or chronologically accurate, but rather to indicate some of the more important considerations involved.

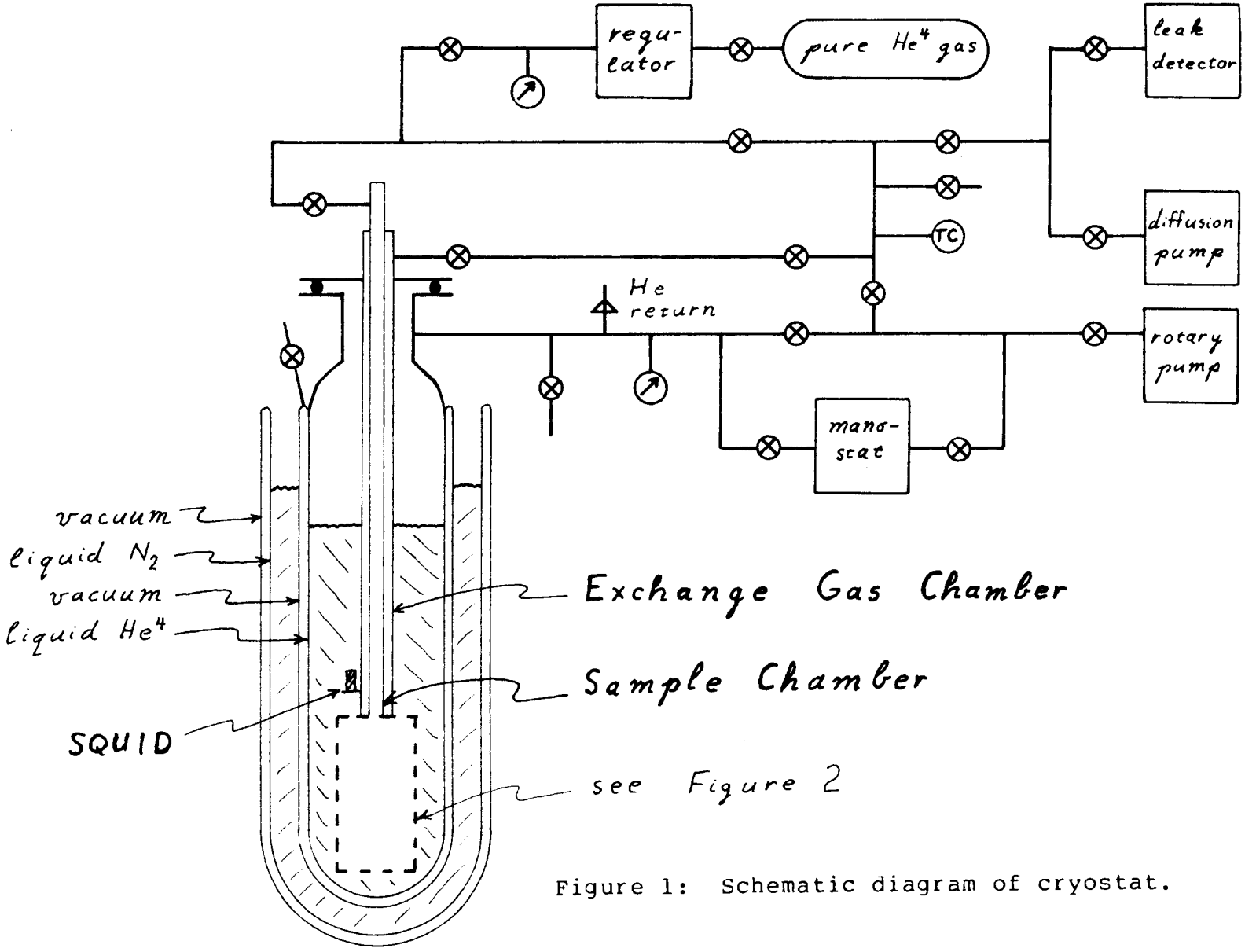

Figure 1: Schematic diagram of cryostat.

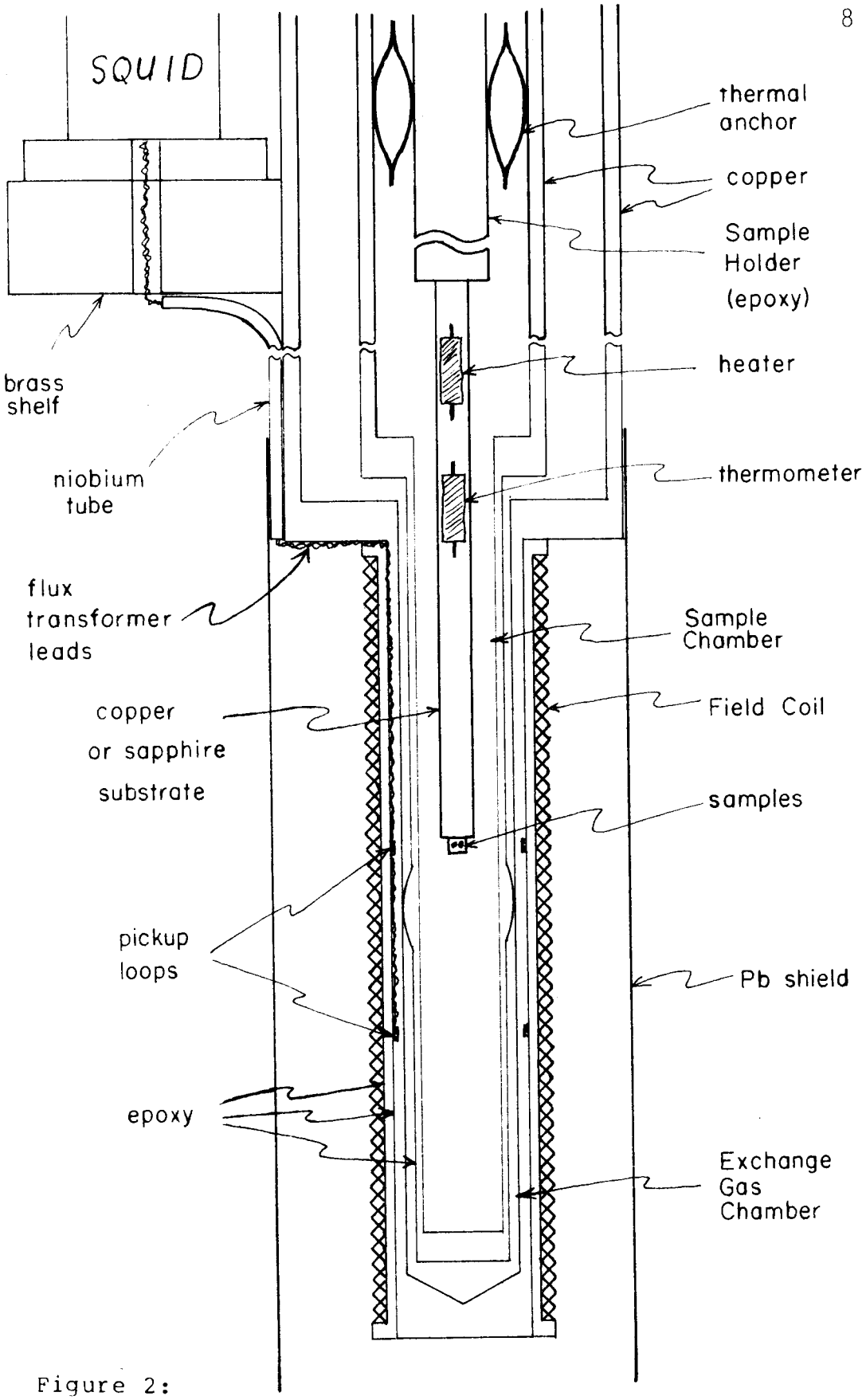

Figure 2:

Lower portion of cryostat. (Approx. twice actual size.)

TEMPERATURE CONTROL: Control of the sample temperature is basically accomplished as follows: The Helium Bath Chamber is pumped to about 1.7K. The Sample Holder is anchored to the bath temperature at a point just above the heater. The Sample Holder is otherwise thermally isolated by evacuating the Sample Chamber to a pressure of about 1 pascal (7.5 microns Hg). The sample temperature can then be swept from the bath temperature up to about 10K by varying the current supplied to the heater.

Several other methods of temperature control were attempted. These all involved the forced condensation of pressurized helium gas in either the Exchange Gas Chamber, or the Sample Chamber. Such techniques cause warming and/or cooling of portions of the walls of these chambers. The signals consequently received by the SQUID, whether due to physical distortions or magnetic transitions, were intolerably large.

HEAT LEAKS: Care was taken to minimize the heat leak into the helium bath so as to reduce helium consumption and increase running time. It is also desirable to avoid any vibration or temperature fluctuations which might be caused by boiling of the liquid. (See discussion of SQUID noise, below.) Note the use of low-thermal-conductivity construction materials such as thin-walled stainless steel tubing and epoxy. Miniature and sub-miniature coaxial cables

were used for cryostat leads in order to further reduce heat leaks.

Even more care was taken to reduce the heat leak into the Sample Chamber. (See the discussion of thermometry below.) Note the use here also of thin-walled stainless steel tubing and epoxy. All wires down the length of the Sample Holder were .08-mm diameter manganin, chosen for their low thermal conductivity. Small brass plates were painted flat black and inserted at intervals in the Sample Chamber. These, as well as the thermal anchor described below, served as radiation baffles.

Total heat leak into the helium bath was kept to about .3 watts, as deduced from the rate of helium evaporation at 4.2K.

THERMAL ANCHOR: The design of the thermal anchor is worth discussing in some detail as it performs two roles of rather crucial importance. The Sample Holder conducts about 10-20mW of heat from room temperature down its length into the Sample Chamber. Such a large flow must be shunted into the helium bath before it reaches the sample or thermometer where it would interfere with temperature control and measurement. The thermal anchor was intended to provide this shunt and also to serve to center the Sample Holder, preventing lateral vibrations. The anchor was made from a rectangular piece of copper sheet measuring about 3 cm (1 1/8 inch) by 8 cm (3 inch) in

area by .1 mm thick. A series of parallel slits were cut in the sheet, each end of each slit stopping just short of the edge of the sheet. The sheet was then rolled into a cylinder 1 cm (3/8 inch) in diameter with its axis parallel to the length of the slits. The cylinder was then crushed lengthwise so as to force the copper to curve alternately inwards and outwards on each side of the slits. The resulting structure fits quite snugly between the coaxial cylindrical walls of the Sample Chamber and the Exchange Gas Chamber.

The advantages of this design are that it makes fairly good thermal contact at all temperatures (unlike a rigid structure) by virtue of its springiness and high thermal conductivity; yet it does not interfere with the free motion of the Sample Holder into and out of the Sample Chamber. It should be noted that some material more springy than copper, such as phosphor bronze or beryllium copper, would probably serve better despite their lower thermal conductivity but these were not readily available in thin sheets.

Since this thermal anchor is positioned so near to the SQUID and to the sample, superconducting or magnetic materials could not be used in its fabrication. This meant also that it had to be fixed in shape and in position by its own elastic tensions rather than with solder.

A slightly more elegant solution to the thermal anchoring problem was found in the form of braided copper electrostatic

shielding which can be longitudinally crushed or stretched to serve in much the same way as the slotted copper sheet. However, it was not possible to obtain this braid without its usual layer of superconductive tinning.

PUMPING LINES: Consideration was given to the diameters and lengths of pumping lines in order that difficulties such as convection, heat conduction, or excessive pressure drops be circumvented. For these purposes a few formulae from Reference 42 are normally sufficient:

The pressure drop along a tube of circular cross section is given by

$$\Delta P = \eta \, z \, \dot{V} \qquad \text{Eq 1}$$

where η is the viscosity of the fluid flowing through the length of tube at a rate of $\dot{V}$. If the tube has length, l, and diameter, d, its impedance is

$$z = \frac{128 \, l}{\pi \, d^4} \qquad \text{Eq 2}$$

In deriving the above expressions, one must assume, among other things, that the flow is non-turbulent (i.e. laminar), that the gas

is at uniform temperature, and that the flow has no net divergence.

The following table of helium viscosity is from Reference 76. One poise is one gm/(sec-cm).

T (K)	η (μpoise)
15.8	27.0
20.6	35.0
81.6	87.1
273	186.0
293	194.1

Table I

Graphs of pressure drop per unit length vs tubing diameter generated from Eq 1, Eq 2, and Table I, are given in Figure 23 in Appendix G.

EPOXY: The "epoxy" referred to above and below is Emerson and Cuming Stycast 1266. (See Note 3.) It was cast, not according to the instructions of the manufacturer, but following the recipe given in Appendix C. The resulting material is transparent, strong, and easily machined. Since it is also electronically and magnetically inert, it was well suited for the construction of the lower portion of the cryostat. However, its large coefficient of thermal expansion makes it difficult to seal reliably to other materials. Data on integral thermal contraction of epoxy could not be found but it is

probably at least 2 to 4 times that of copper, between room temperature and 4.2K. This drawback caused some rather disappointing vacuum failures in the first version of the cryostat. The problem was finally overcome using a technique described by Wheatley in Reference 67. The epoxy-metal joint shown in Figure 3 was made according to Wheatley's suggestions. Notice the very thin wall of the epoxy section. These seals seem to be remarkably strong and have withstood pressure differences, both under compression and under expansion, of up to two atmospheres at temperatures ranging between 1.5K and 300K.

A point worth noting in connection with epoxy is that it was found to be permeable to helium gas. Samples of Stycast 1266 were made in the form of cylindrical shells of assorted wall thicknesses ranging from 15 mils to 50 mils. These were connected to a leak detector and exposed to an external pressure of 1 atmosphere of helium gas. The rate of helium leakage was found to increase from zero to about 10^{-12} moles/sec (10^{-7} std cm^3/sec) over a period of about one minute at room temperature. This time constant increased as sample thickness was increased. Samples over about 1mm (39 mils) in thickness leaked negligibly. Since the rate of helium leakage decreased rapidly as the sample was cooled and was negligible below about 200K, it was assumed to be a diffusion effect. Dependence of

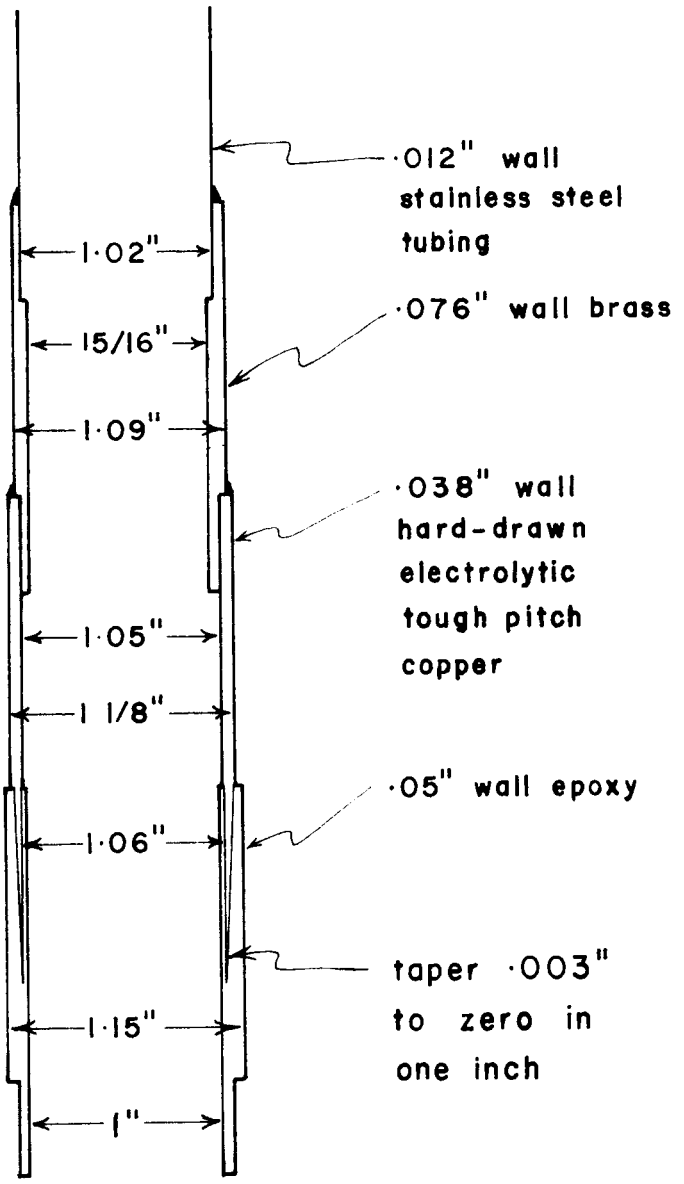

Figure 3: One of the two epoxy-to-metal vacuum seals used in the cryostat.

diffusion rate upon thickness was not established, due to lack of reproducibility in the quantitative results. Nevertheless, it was ascertained that the leak rate varied with temperature like e^{aT} where $a = .05\text{-}.09/K$. This behaviour must be kept in mind when using helium around epoxy parts at room temperature. Zimmerman (Reference 72) also has observed helium diffusion through the walls of his epoxy dewars.

MISCELLANEOUS: Careful calculations were made of the rate of heat flow in various portions of the cryostat, especially in the region of the Sample Chamber. Such calculations are reasonably straightforward in most cases and Reference 9 was quite helpful for these problems. However, the case of two surfaces separated by a distance comparable to the length of the mean free path of the exchange gas between them can be a particularly sticky one. It is usually better to avoid the situation by adjusting the geometry or the pressure. Plots of the mean free path of He^4 gas are helpful for this purpose. See Figure 22 in Appendix F.

Reference was made to several of the standard texts (References 30,45,55,68) on low temperature experimental techniques.

Invaluable data on properties of materials which are useful to the experimentalist were found in References 30,37,45,54,55,68,69, 75,76.

A formula useful for the calculation of the inductances of the various coils used was found in Reference 29:

$$L = \frac{r^2 n^2}{23r + 25l} \times 10^{-6} \text{ henry} \qquad \text{Eq 3}$$

where r = coil radius in cm

l = coil length in cm

n = number of turns

The usual precautions were taken to avoid the use of excessively corrosive flux in assembly of the cryostat in order to prevent corrosion-caused vacuum leaks. All surfaces of the cryostat were carefully cleaned after soldering, so as to remove any flux remnants. This was done also in order to remove any flakes of solidified flux, oxides or other garbage which might fall into the pickup loops in the bottom of the cryostat.

A product called Sta-Lok was found to be invaluable. It can be applied to almost any small, room-temperature vacuum leak to seal it immediately, in situ, without the need for disassembly, curing or soldering. Sta-Lok is obtainable from Broadview Chemical Corp., Broadview, Illinois.

SQUID

INTRODUCTION: The SQUID system used was the fairly standard rf-biased point-contact configuration. The SQUID itself was manufactured by S.H.E. Corporation of San Diego, Calif. Figure 4 shows two cross-sectional views through the device. Figure 5 shows the home-made assembly with which the SQUID was mounted on the cryostat.

The SQUID can be thought of as a superconducting loop circuit containing a Josephson junction, or "weak link". This loop is inductively coupled to a resonant LRC tank circuit. The inductive load offered by the SQUID is sensitively dependent upon the status of the weak link, which, in turn, depends periodically upon the number of flux quanta threading the superconducting loop. In practice, this periodicity is often removed by operating the SQUID in the feedback, or flux-locked loop, mode shown in Figure 6. With this arrangement, the detector output is directly proportional to the flux coupled into the SQUID. The flux transformer shown in the diagram is nothing more than a superconducting loop which acts as a DC transformer magnetically coupling the sample to the SQUID.

Fairly detailed mathematical treatments of the theory of operation of SQUID's can be found in References 19,27,37,45, among others. The reader is referred to Reference 72 for an example of a

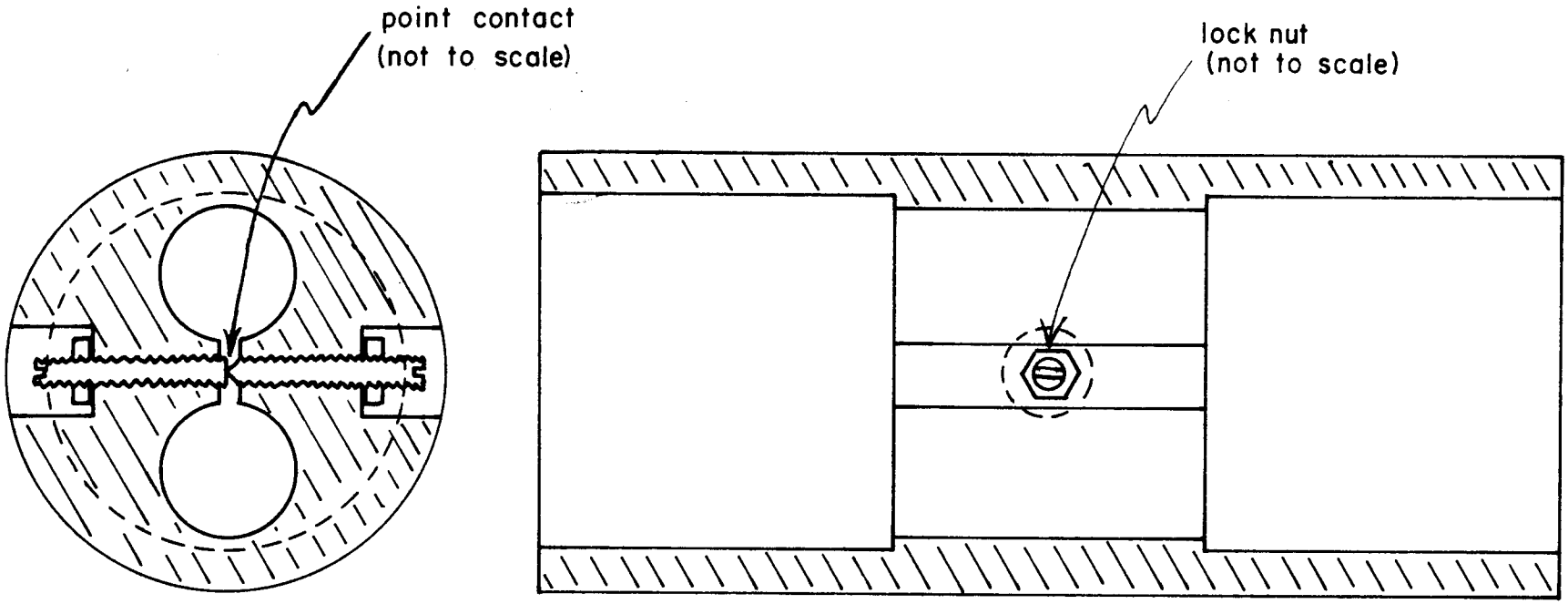

Figure 4: Two cross-sectional views through center of a two-hole point-contact SQUID. (Approx. 10 times actual size.)

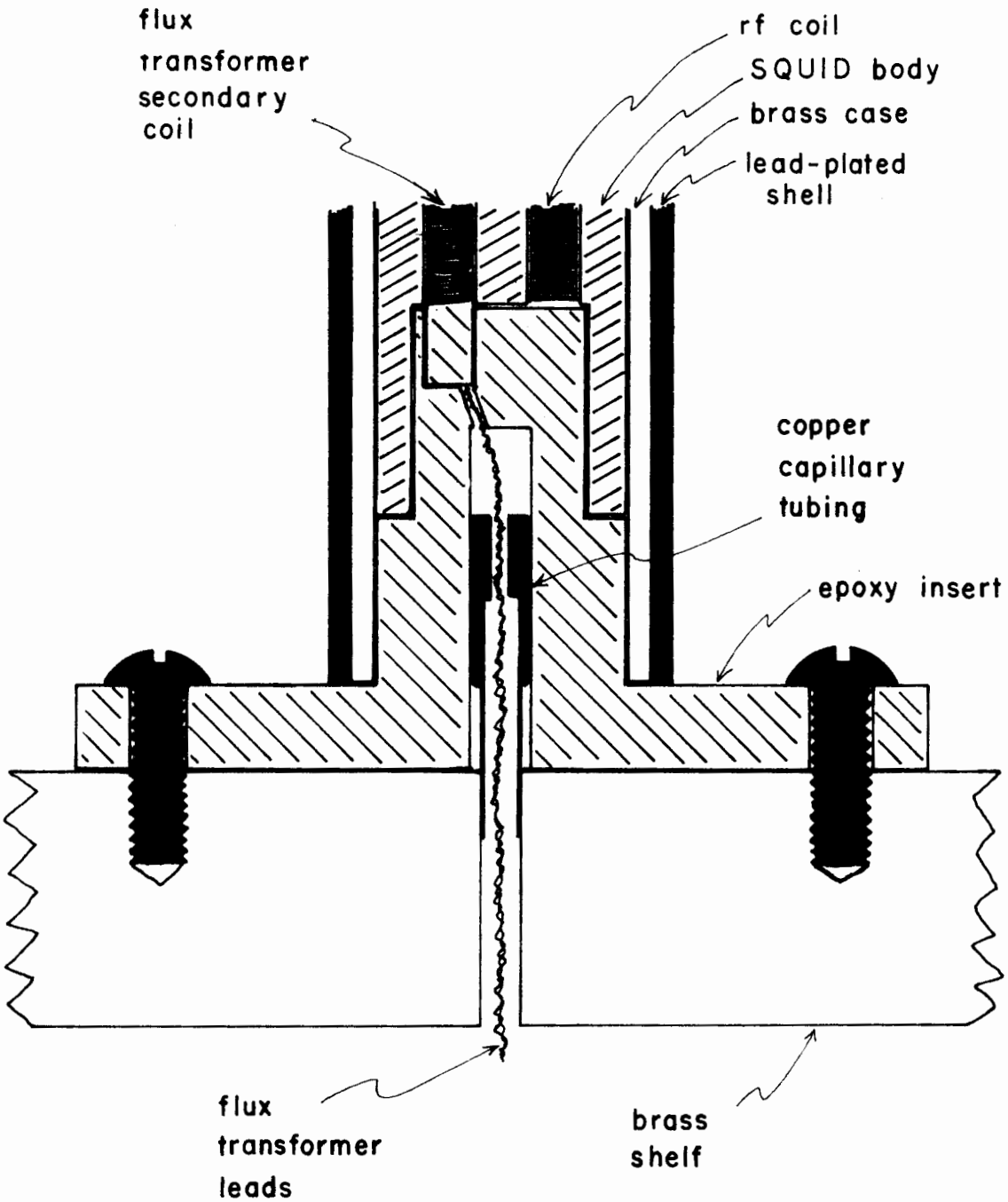

Figure 5:

SQUID mounting assembly. Can be made vacuum-tight by sealing copper tubing with epoxy.

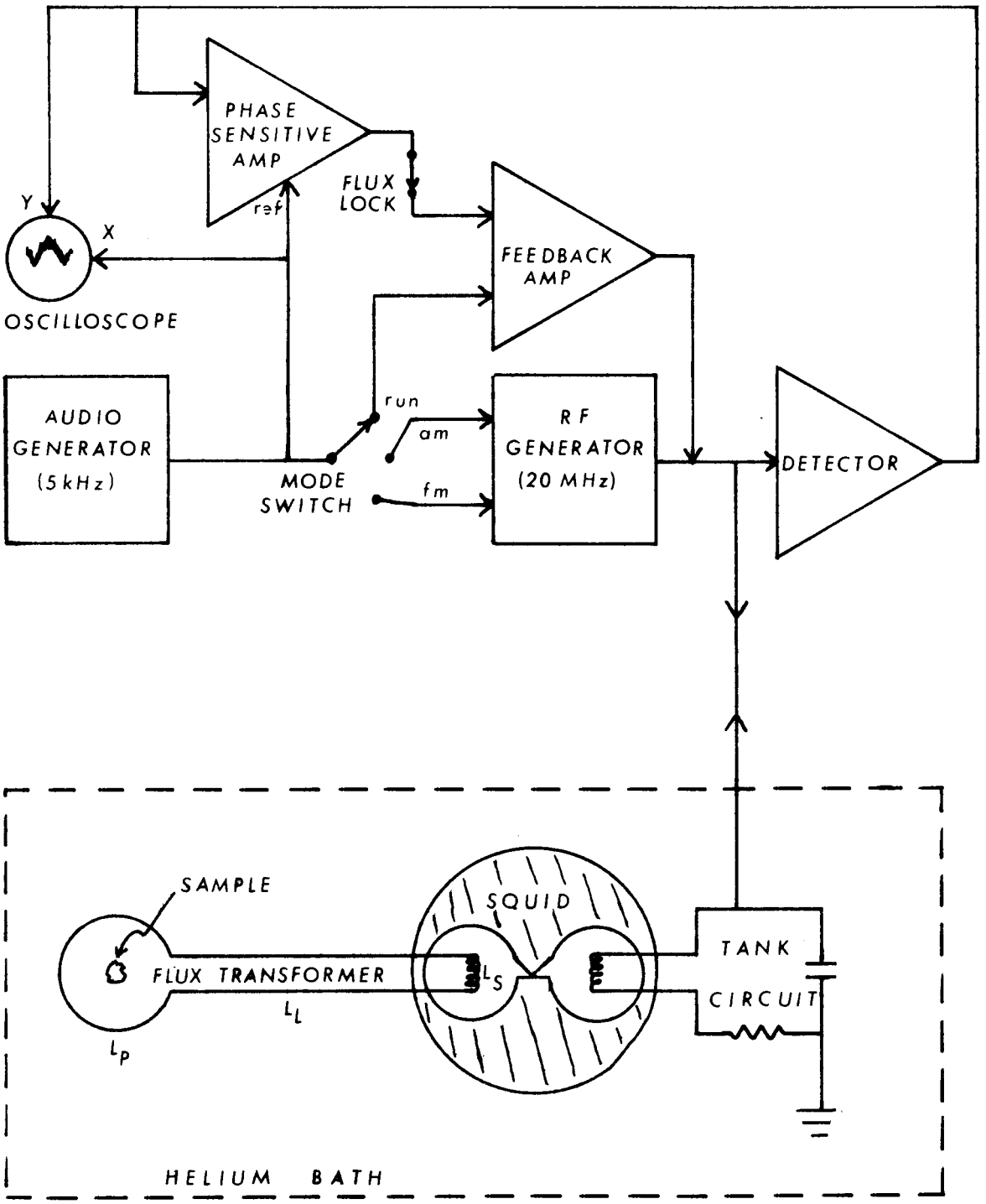

Figure 6: Typical RF-biased SQUID system.
Shown in flux-locked mode.

more intuitive approach which avoids the rather tedious mathematics of a rigorous model.

FLUX TRANSFORMER: The flux transformer was designed following the discussions in References 27 and 45. It was wound from .076-mm (3-mil) diameter niobium wire. (See Note 2.) The necessary splices were made with spot-welds. Screw-contacts were also tried but were found to be quite noisy, due to the admission of stray flux into the circuit, even when great care was taken to make them compact enough to eliminate included area.

The most obnoxious property of the flux transformer was the propensity of the wire for breaking for no apparent reason. This problem was particularly annoying as it was never detected until the cryostat had been cooled to 4.2K. It seemed that, if the coil was wound tightly, the differential thermal contraction of the niobium and the epoxy around which it was wound broke the wire, while if the coil was wound loosely, the wires would vibrate and break due to their brittleness when cold. The solution to the problem was as follows: The coil was wound with enough slack in it to accommodate the differential thermal contraction of the niobium and its epoxy coil form. Then the wire was smeared with a layer of vacuum pump oil. The oil solidifies at a temperature low enough that much of the

thermal contraction has taken place, and then acts as a cement to prevent the wire from vibrating and breaking when the wire is brittle. Similar wire breakage problems were encountered elsewhere in the cold portions of the apparatus where wires had been permanently glued to substrates with incompatible thermal expansion coefficients.

As can be seen from Figure 2 (p8), the diameter of the pickup coil is much larger than the sample dimensions. Thus the coupling between the sample and the pickup loop is quite poor, resulting in a reduction of the signal by a factor of about 100. This situation could be greatly improved by making the pickup loops smaller but this would involve running the wires through the wall of the Exchange Gas Chamber. Then, if the pickup loop broke, major reconstruction would be involved. It was felt that the additional complications were not warranted.

CRYOSTAT CONSTRUCTION MATERIALS: Obviously, the pickup loops must be shielded from varying magnetic fields as these will produce signals which may render invisible the signal of interest. Virtually any metal will have magnetic impurities which may give large field-dependent signals. There might also be troublesome eddy currents established in metal parts. In order to avoid such problems the lower portions of the cryostat were made of epoxy, which is known

to be magnetically and electronically "inert".

Solder joints and indium vacuum seals can cause difficulties too. Such seals usually take the form of a ring or loop and therefore exhibit large field-dependent magnetic moments when in the superconducting state. (In fact, superconducting materials in general should be avoided due to their diamagnetic behaviour.) Special care was taken to avoid having these loops anywhere near the SQUID or the sample. One solder loop was used in the lower portion of the Exchange Gas Chamber outer wall but, since the loop was immersed in the constant temperature liquid helium bath, and was located at some distance from the pickup loops, its effects were not noticed.

AMBIENT FIELDS: The earth's magnetic field displays low frequency (4 Hz and less) oscillations with typical amplitudes of 10 micro-gauss (Reference 72). These are well within the SQUID's limit of resolution and must be guarded against. This problem was solved by enclosing the SQUID and the flux transformer within superconducting shields (lead and niobium were used) as can be seen in Figure 2 (p8). The oppositely-wound pickup loops used also reduce sensitivity to such variations.

Movement of magnetic or metal objects within a distance of a few

meters of the cryostat was observed to cause significant signals. Even motion of the experimenter near the cryostat was easily detectable. It was felt that this latter effect was attributable to a few unavoidable ground loops and coupling of the experimenter's body to them. For these reasons movement of anything near the cryostat was not permitted during an experimental run.

VIBRATION: Vibration is often the most serious source of noise in SQUID-based systems as it can lead to induced currents in both normal and superconducting components if there are spatial variations in the applied magnetic field. Even the boiling of the liquid helium bath and the flutter of the one-way valve in the helium recovery line were observed to cause detectable signals. Therefore some trouble was taken to make certain that the whole cryostat was structurally rigid and mechanically isolated with flexible pumping lines. As previously mentioned, the thermal anchor served to secure the Sample Holder in its chamber. Glass wool was tightly stuffed between the Sample Chamber and Exchange Gas Chamber walls. A simple conical cardboard collar was used to center the whole assembly in its glass dewar. Large metal objects, like helium dewars and equipment racks, were kept as far away as possible to avoid any non-uniformities which they might introduce into the ambient field. (See Reference 73.)

ELECTRICAL NOISE: Sources of electrical noise such as rf and line frequency signals were carefully guarded against by strictly adhering to good grounding practices and carefully shielding all leads. All SQUID leads were doubly shielded.

Some workers in the field (Reference 27) stress the necessity of installing filters on all leads into the cryostat to exclude any stray rf signals which would bother the SQUID. For this reason all cryostat leads were shorted to ground through 100pf capacitors. However, these were subsequently removed as they had no noticeable effect upon the SQUID noise level and introduced troublesome time constants into other circuits. By far the major component of the SQUID noise was 60Hz line frequency (about 1/2 flux quantum peak-to-peak) with lesser contributions (about .03 flux quantum peak-to-peak) from the gating signal (and its higher harmonics) of the phase sensitive detector. Noise was measured at the detector output in the lock mode. The source of the 60Hz noise could not be precisely determined but it appeared to arise from poor isolation of power supplies and some ground loops. These problems are intrinsic to the equipment used and could not be rectified without major reconstruction of same.

TEMPERATURE STABILITY: Temperature stability is important not only for solder joints but also for the SQUID itself and the flux transformer. Since the SQUID is used in a flux-locked configuration, the measured signal is not sensitive to SQUID temperature. However, the rf level at which the SQUID operates does vary with temperature. (See Figure 7). Therefore fluctuations in the SQUID temperature can degrade the stability of the flux-locked loop and are to be avoided if possible. Accordingly, the SQUID and the flux transformer were mounted in the helium bath which was maintained at constant temperature throughout the experiments.

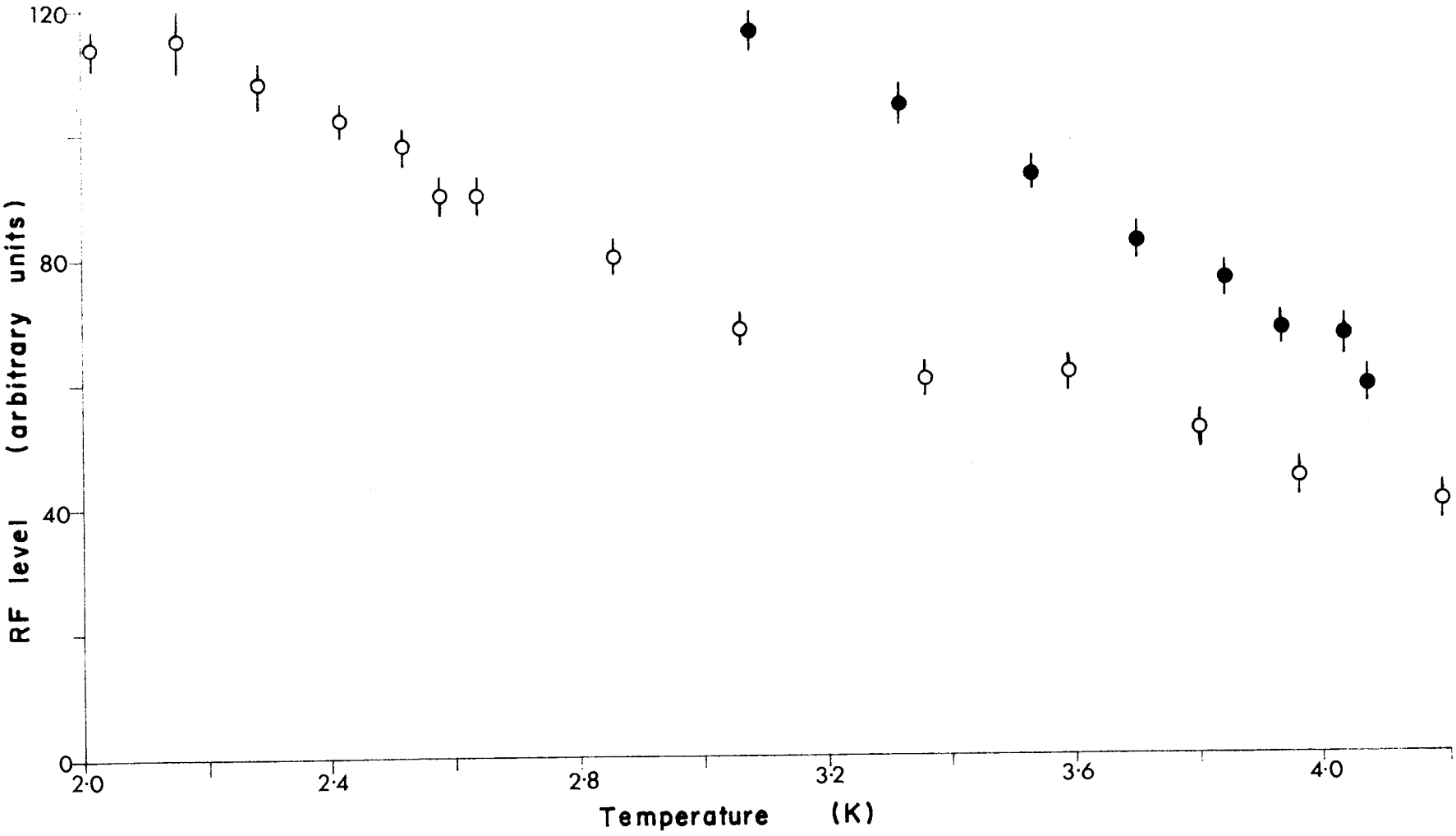

Figure 7: Optimum RF level for operation of our SQUID. The two sets of points correspond to data collected while cooling the helium bath on two different days.

FIELD COIL

The tremendous sensitivity of the SQUID also demands great stability in the applied fields. The two pickup loops are nominally identical, but wound in opposition so as to be insensitive to the magnitude of the applied field and measure only the component of its gradient which lies along the axis of the loops. Since it is unlikely that the loops will be absolutely identical, one can wind also a compensation coil around one of the pickup loops. A small fraction, f, of the current flowing to the field coil is shunted through the compensation coil so as to cancel the out-of-balance signal observed when the field current is varied. This was done, and, as a further precaution, two 12-volt automobile batteries in series were used to supply the field current so as to minimize introduction of line noise. It was found, however, that these measures were inadequate. The value of f needed to compensate the field dependence of the SQUID signal was small (about .01, or less), but seemed to vary with time and with field. This may have been caused by physical distortions of the coil when the field was changed or by interaction with nearby superconducting or magnetic materials. Regardless of the cause, this meant that it was not, contrary to original expectations, possible to produce magnetization vs field curves. As a consequence, all data were collected in constant field.

It is a dramatic illustration of the sensitivity of the SQUID system that there were occasions on which the exponential decay of the field current due to loading of the car batteries produced a signal many times larger than the signal of interest. This was with fully charged batteries and a load of only 10mA. Although some data were collected in spite of this problem the compensation approach was eventually discarded. It was found to be much more satisfactory to install a heat switch and use the field coil in a persistent current mode:

The heating element of the heat switch is a 10-kilohm metal-film resistor. A length of about 30 cm of superconducting wire (see Note 1) was folded in half and then tightly wound around the body of the resistor. This minimizes the mutual inductance of the two while maximizing thermal contact. The resistor was then painted with GE varnish and potted with melted vacuum grease in a small receptacle machined from epoxy. The result is a rather neat package with four leads coming out for connection to the rest of the circuit. The epoxy provides a degree of thermal isolation for the heater. The use of grease and GE varnish for potting allows the heat switch to be taken apart for repair or alteration. Such a heat switch requires 2-5mA to drive the superconducting wire into the normal state, in which it has a resistance of about 40 milli-ohms. The heat switch is

controlled with a rheostat instead of a switch, thereby minimizing transient signals induced by the operation of the heat switch.

Prober (Reference 50) also encountered problems related to high field measurements using a SQUID.

THERMOMETER

Temperature measurement was accomplished by means of conventional carbon resistance thermometry. The resistors used were 1/4 watt 200 ohm carbon composition resistors manufactured by Speer Electronic Components, Bradford, Pennsylvania. The resistors were used unaltered, except that the leads were shortened to about 3 mm and all traces of tinning carefully scraped off. Wires were soldered to the leads using Wood's Metal. Because of its low melting point, Wood's Metal can be used to solder wires to the resistor without heating it to the point at which its resistance versus temperature behaviour might be altered.

Wood's Metal is superconducting at temperatures below about 8K and therefore can give rise to the field-dependent signals mentioned earlier. A low-melting point solder with a superconducting transition temperature below 1.6K would have been a better choice. However, it was found that the magnetic moments of these Wood's Metal joins were small enough and far enough from the pickup loops that their effects were negligible.

The thermometer resistance was measured with a four-terminal DC setup (see Figure 8). Power dissipated in the resistor was kept below 10 nW. The potential drop across the thermometer was measured with both polarities of current flow and an offset was applied to

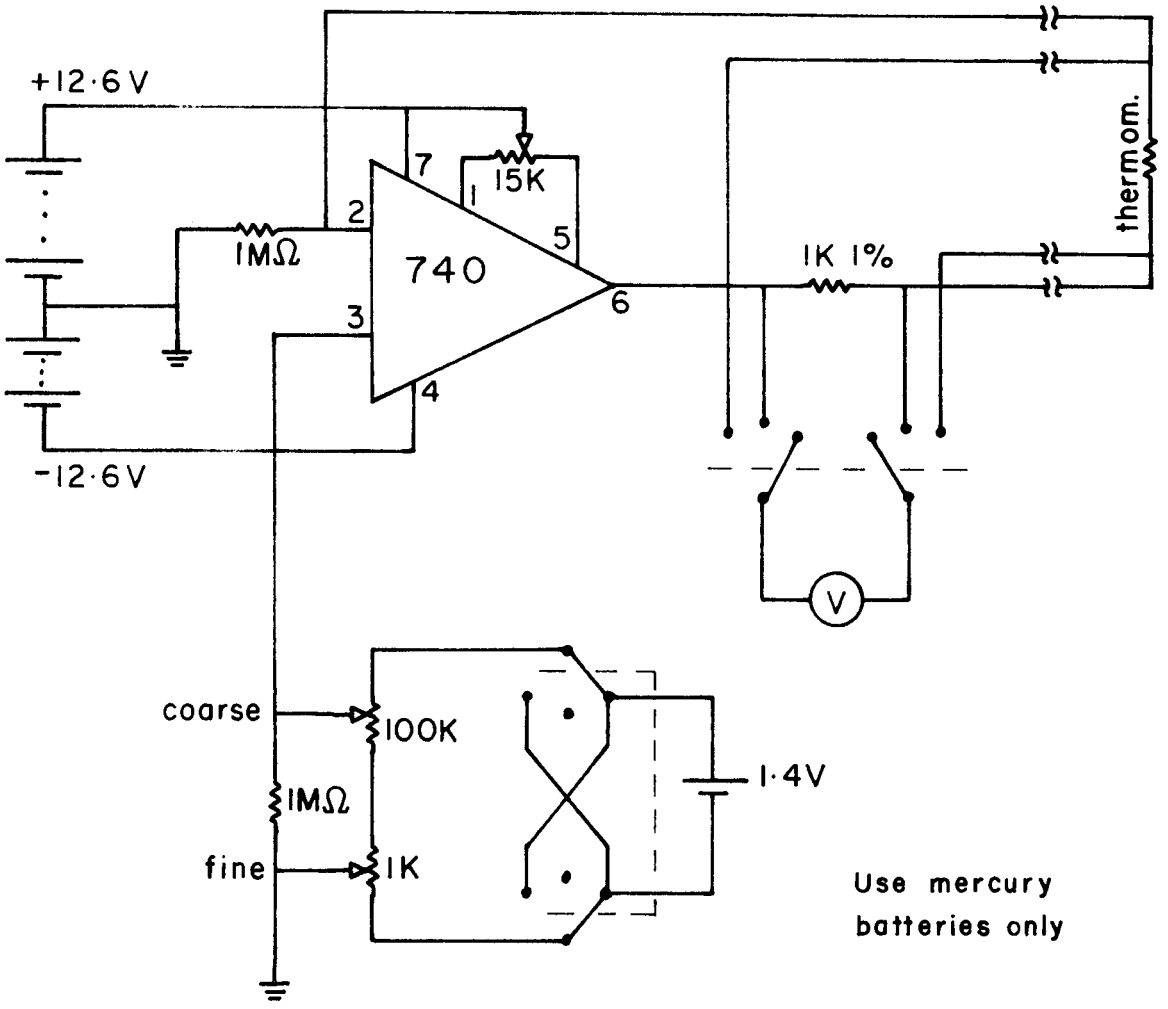

Figure 8:
Constant current power supply used in four-terminal arrangement for resistance thermometry. Voltmeter (V) is a Keithley 147 Nanovolt Null Detector.

eliminate the effects of thermal emf's. The thermometer was calibrated against the 1958 He^4 scale of temperatures (Reference 75) by dangling it in an evaporation cryostat, giving a set of points T_i (in K) and R_i (in kilohms). The data was broken into three intervals and was "fitted" (in the least squares sense) to a curve of the form

$$\frac{1}{T} = A + B\log_{10}R + C(\log_{10}R)^2 \qquad \text{Eq 4}$$

over each of the intervals. The optimum choice of intervals was found as follows; The data was first fitted by a curve of the above form over the single interval from 1.6K to 4.2K. i.e.

$$T_1(R) = [A_1 + B_1\log_{10}R + C_1(\log_{10}R)^2]^{-1} \qquad \text{Eq 5}$$

The residuals, $T_i - T_1(R_i)$ were then plotted vs $\log_{10}R_i$. This curve displayed the often-seen (Reference 28) oscillatory behaviour shown in Figure 9. Each half-cycle of oscillation was designated as one interval for the purpose of making the final fit. The intervals were overlapped by one or two data points to help smooth the fit. The residuals, $T_i - T_3(R_i)$, of the final 3-interval fit are plotted in Figure 10.

Several methods for fitting the calibration points to several

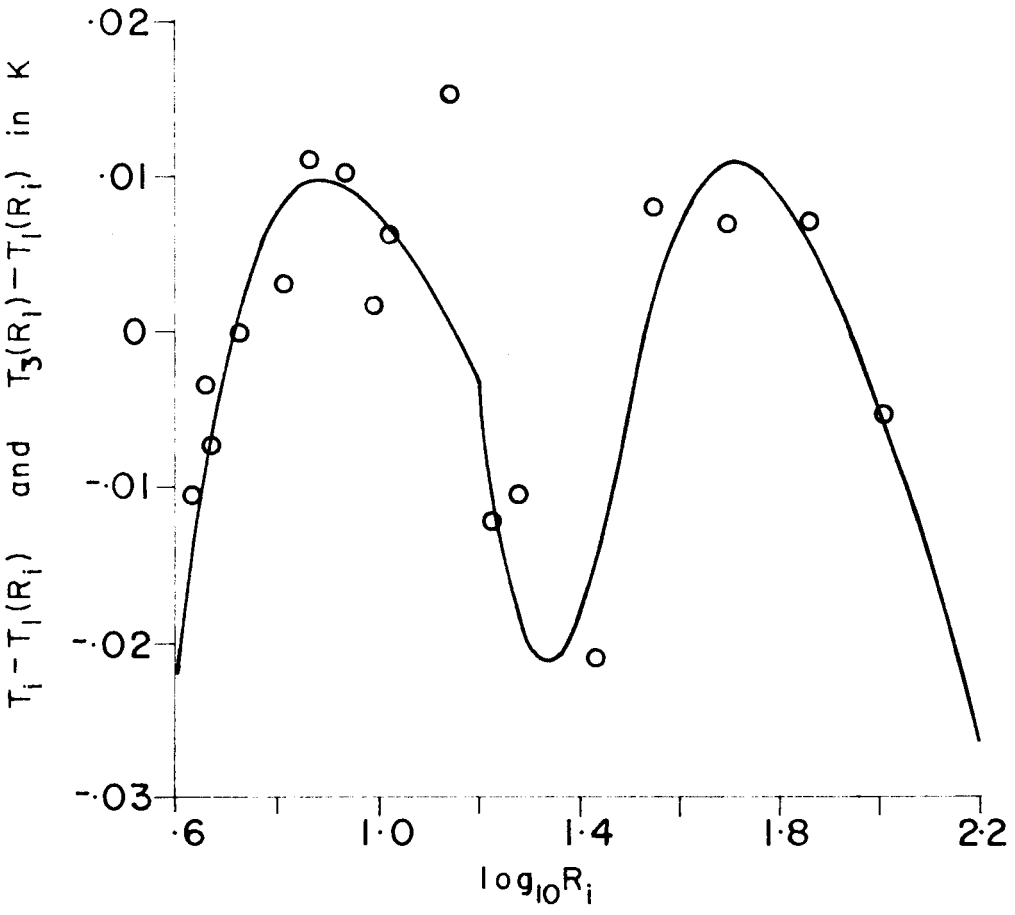

Figure 9:

Residuals (circles) of single-interval thermometer curve fit. Solid curve is $T_3(R_i)-T_1(R_i)$, the difference between the 3-interval fit and the single-interval fit.

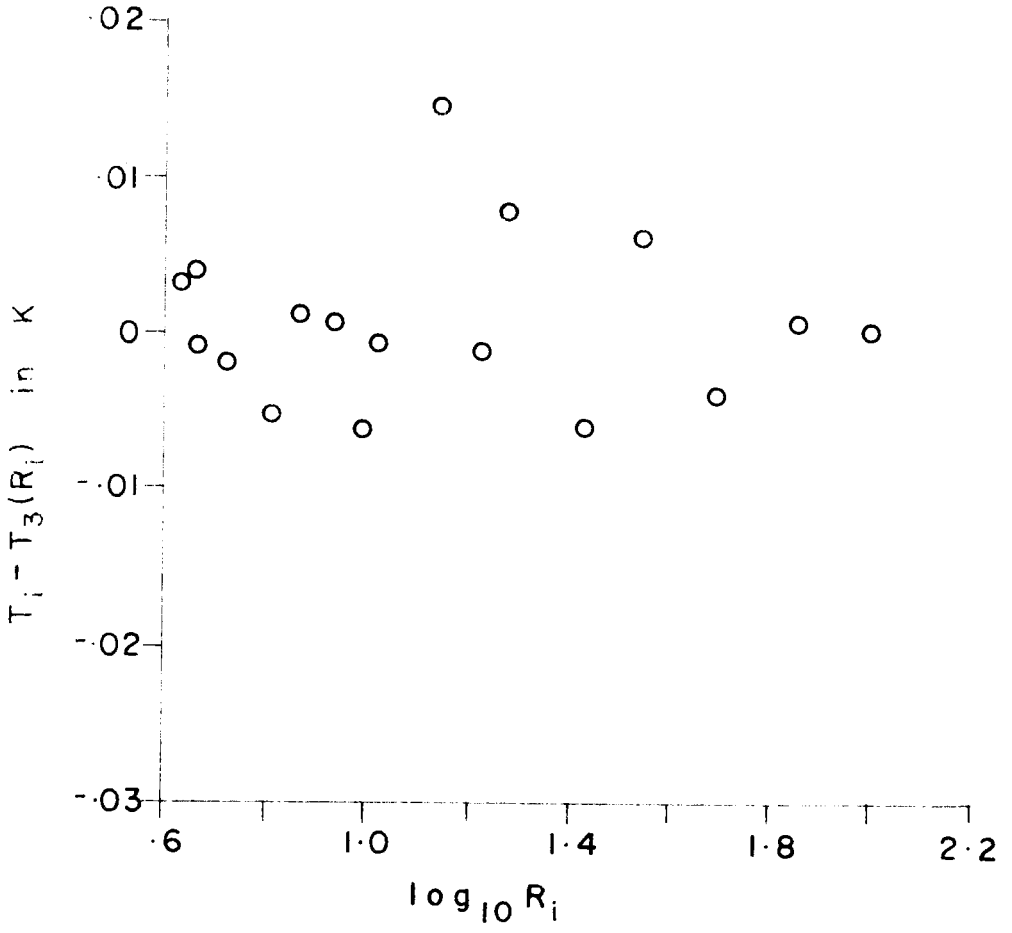

Figure 10:

Residuals of the final 3-interval fit for one (R_D) of the two thermometers used.

different functional forms were tried, but the above method was found to be the most satisfactory. It should be noted that curve fitting techniques are often applied giving no consideration to whether or not the fit is "ill-conditioned" (see Reference 10). If the fit is ill-conditioned a large number of significant figures may have to be carried in the coefficients A, B, and C of Eq 4 to prevent round-off error from having disastrous effects. This was taken into consideration in the choice of the most satisfactory fitting technique. Consideration was also given to ease of application and calculation of the fit.

This particular brand of resistor seems to be well-suited for thermometry. The resistance versus temperature behaviour is remarkably similar for different individual resistors. They also do not seem to suffer any ill effects from repeated thermal cycling between 1.5K and 300K, as do some resistors. The calibration of one thermometer was checked after several thermal cycles and calibration points were found to be reproducible within experimental error (.3% in resistance and .5% in temperature). However, as previously mentioned, care was taken to avoid heating these resistors much above room temperature.

SAMPLE PREPARATION

Samples of $TaS_2(aniline)_{3/4}$ were obtained from A.H. Thompson, Exxon Research Labs, Linden, N.J. The TaS_2 from which they were prepared was crystalized by the iodine vapour transport technique (Reference 15), in the presence of excess sulphur. These samples are from the same batch (SU-1) as those used by Gamble et al (Reference 23) and by Prober (Reference 50).

Dimensions of the samples observed are given in the table below. Volumes were calculated from the density and the measured weights. Thicknesses were measured under an optical microscope. A range of values indicates a variation in thickness within the sample. The area quoted is simply the ratio of the other two quantities. Those samples designated as "cleaved" were made by using adhesive tape to cleave a larger as-grown intercalated crystal.

sample #	cleaved?	thickness(cm)	area(cm^2)	volume(cm^3)
6	no	.02-.03	4-6 $x10^{-3}$	122.7 $x10^{-6}$
10	no	.02	4 "	81.19 "
16	no	.003	.5 "	1.6 "
19	yes	.006-.01	10-17 "	101.6 "
20	yes	.006	4 "	25.13 "
21	no	.01	3	34.6 "
24	yes	< .002	> 8 "	16.04 "
25	yes	.01	8 "	77.27 "
26	yes	.01-.02	7-14 "	146.3 "
27	yes	.02-.03	15-22 "	447.0 "

Table II

Three samples were mounted for each experiment; one of indium or tin, one of thallium, and one of the unknown. The known samples served as temperature markers as a cross-check against the resistance thermometry. The markers used were initially all at least 99.999% pure. They were etched in nitric acid and pounded to a thickness of about 20 microns between two sheets of polyethylene. They were then etched again and washed in ethanol. A razor blade was used to cut the markers into pieces about .5 mm square, while still immersed in alcohol. Finally, they were mounted using a thin coat of L grease on both faces of the samples. These precautions were mainly for the benefit of the thallium, which oxidizes readily. In fact, the thallium samples had to be replaced frequently because oxidation had broadened their superconducting transitions.

SAMPLE SUBSTRATE

The thermometer, heater, and samples were all mounted on a thermally conductive substrate as shown in Figure 2 (p8). Due to the high sensitivity of the SQUID magnetometer, the substrate must be made of a material which is magnetically and electrically inert. The heater and thermometer must be mounted a sufficient distance away from the pickup loop for the same reason, making it especially important to use a substrate material of high thermal conductivity in order to maintain good thermal contact between the sample and the thermometer. Over the temperature range from 1.5K to 4.2K (and higher) sapphire makes a good substrate. It was later found that oxygen-free copper could also be used with success. Thermal contact between the thermometer and the substrate was made by lashing the two tightly together with thin bare copper wire. A light coating of GE varnish was then applied and allowed to penetrate the lashing and any gaps left between the thermometer and the substrate. The samples were stuck to the substrate with a thin film of Apiezon L vacuum grease. The thermal impedance between the thermometer and the samples was of the order of .01 K/mW.

Neither the indium nor the tin samples posed any problems but thallium was not an entirely satisfactory choice for a marker. Thallium oxidizes rapidly enough to be of some nuisance. The metal

is also quite toxic and contact with the skin is to be avoided (Reference 76). In addition, the superconducting-normal transition of thallium overlaps that of $TaS_2(aniline)_{3/4}$, which makes data analysis a bit more difficult than it might otherwise be. There are no superconducting elements with more desirable properties but InTl alloys can be made with suitable transition temperatures (Reference 57). Such an alloy was cast but found to have a broad transition. Moreover, its transition temperature would have to be experimentally verified for it to serve as an accurate marker. Therefore it seemed simpler to use thallium.

DATA PROCESSING

THERMOMETRY: Data was collected in the form of X-Y recorder plots of SQUID feedback signal, V_S, versus thermometer resistance, R. An example is shown in Figure 12. These plots were then digitized manually for further processing.

The thermometer resistance was converted to a temperature using the interpolation curves mentioned above and given in Appendix E. This temperature we will call T_R (for carbon resistor), to distinguish it from the sample temperature T_S. Since the thermometer could not be mounted near the pickup loops and samples, we are now confronted with the problem of estimating T_S, given only the measured quantity T_R.

Referring to the diagram of the cryostat in Figure 2 (p8), one can construct a simple model for the heat flow patterns in the Sample Chamber. Such a model is shown schematically in Figure 11.

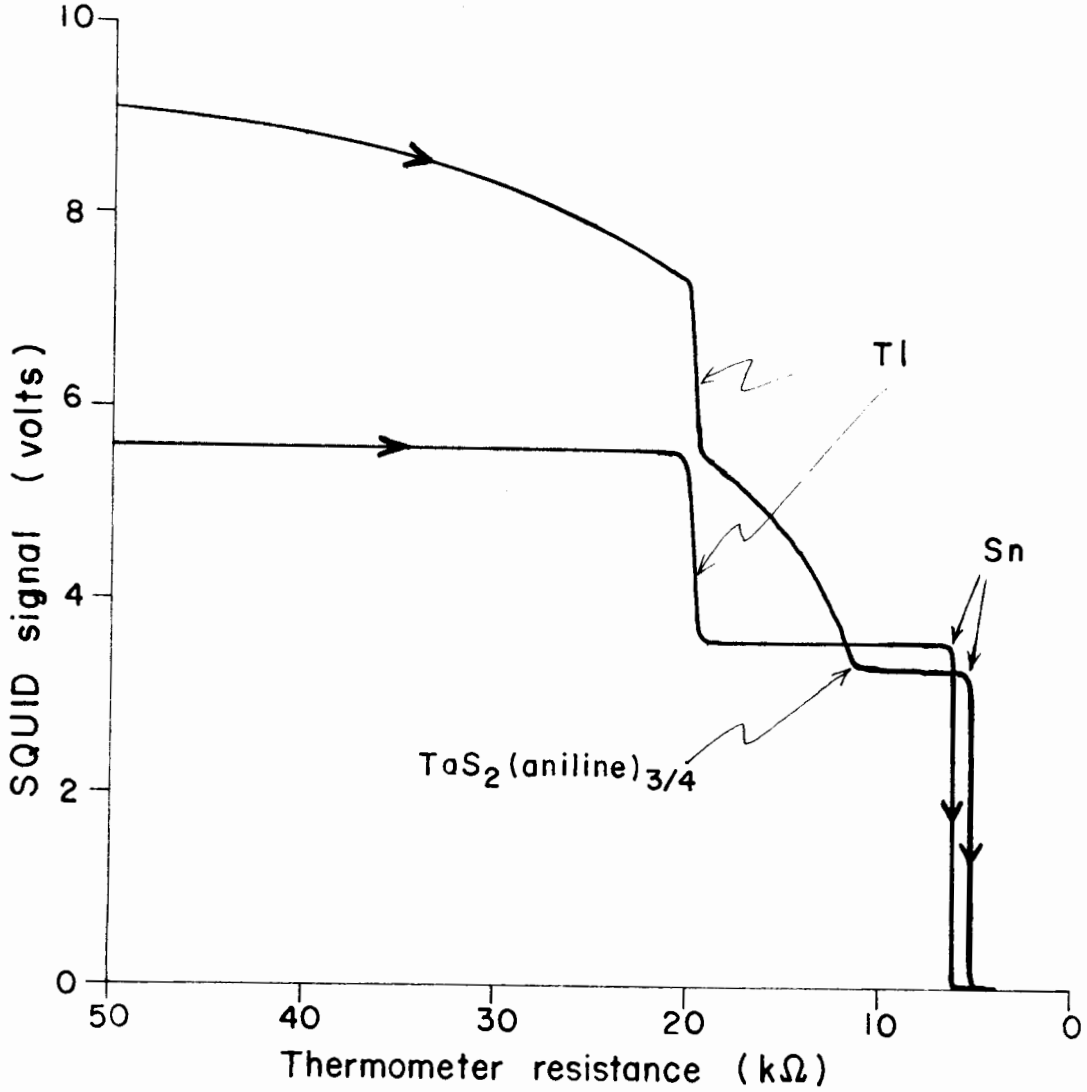

Figure 12:

Typical raw data plots. These curves are shown as illustrations of the appearance of the raw data. One curve represents a temperature sweep with $TaS_2(aniline)_{3/4}$ sample #25, plus marker samples, in a field of 5.25 gauss applied parallel to the layers. The other curve represents Sn and Tl marker samples alone, under the same conditions. Note that the temperature axes (horizontal) do not exactly coincide.

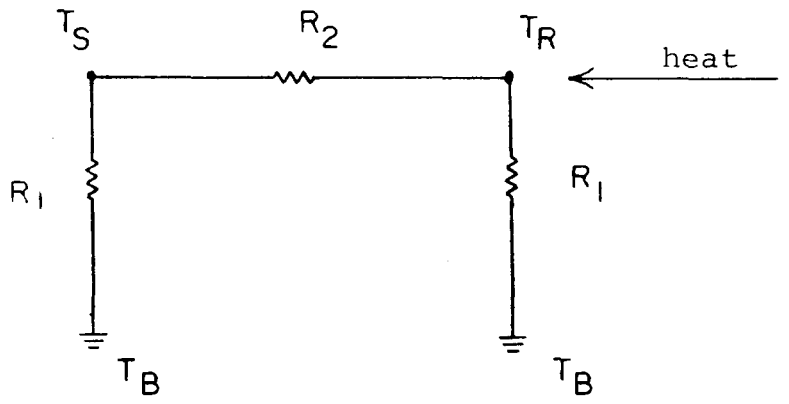

Figure 11

R_2 denotes the thermal impedance between the sample and the resistance thermometer. R_1 represents the thermal impedance between any point on the substrate and the helium bath at temperature T_B. For a high thermal conductivity substrate like sapphire or copper, and with the low gas pressure ($\sim 10^{-5}$ mm Hg) which was maintained in the Sample Chamber, we have $R_2 \ll R_1$. (See Reference 9 and mean free path plots in Figure 22 in Appendix F.) Therefore, by symmetry, R_1 must be the same for all points along the sample substrate.

Applying elementary circuit analysis, we have the result

$$\Delta T = T_R - T_S = \frac{R_2}{R_1 + R_2}(T_R - T_B) \qquad \text{Eq 6}$$

or,

$$\Delta T \simeq \frac{R_2}{R_1}(T_R - T_B) \qquad \text{Eq 7}$$

Moreover, we are in a regime of pressure and temperature such that R_1 is determined by the physical dimensions of the Sample Chamber and can be regarded as independent of temperature.

The temperature dependence of R_2 varies with substrate material. In this temperature region, the thermal conductivity of a metal is characteristic of a free-electron gas while phonons are the dominant mechanism of heat conduction in an insulator. Accordingly,

$$R_2 \sim \frac{1}{T_R^3} \qquad \text{Eq 8}$$

for the sapphire substrate, and

$$R_2 \sim \frac{1}{T_R} \qquad \text{Eq 9}$$

for the copper substrate.

Here we have assumed that ΔT is small enough that temperature differences along the length of the substrate can be disregarded for the purpose of calculating R_2.

Combining the last three equations, we have

$$\Delta T = \frac{a}{T_R^2} + \frac{b}{T_R^3} \qquad \text{Eq 10}$$

for sapphire, and

$$\Delta T = a + \frac{b}{T_R} \qquad \text{Eq 11}$$

for copper, where a and b are constants which were determined by a least-squares fit to three points.

Two points were taken from the observed transition temperatures of the marker samples. The observed transition temperature, T_R, was defined, following Reference 12, as the observed thermodynamic transition temperature - that is, the point of intersection of a line drawn tangent to the steepest portion of the magnetization curve with the line defined by magnetization = zero. This definition is illustrated in Figure 19. The actual $T_C = T_S$ is given with a high degree of accuracy by the familiar empirical equation

$$H_C = H_0\left[1 - \frac{T^2}{T_C^2}\right] \qquad \text{Eq 12}$$

where H_C is the applied field and $T_C(H=0)$ and H_0 were taken from References 37 and 54:

	Sn	In	Tl	
$T_c(H=0)$	3.722	3.409	2.38	K
H_0	309	282	177	gauss

Table III

Due to the finite experimental error of the data points, and the inverse-T_R-dependence of the fitting functions (Eqs 10,11), the fitted curve for ΔT can be very ill-behaved for low T_R. For this reason it was deemed reasonable to add a third fixed point. This last point was manufactured simply by assuming that $\Delta T \equiv 0$ for T_R = 1.5K. Physically, this amounts to saying that the sample and thermometer are initially at the same temperature, within experimental error, before the application of heat from the heater at the start of a temperature sweep.

One might argue that the above theoretical treatment of the heat flow patterns is deficient in that it does not accurately represent the true distributed nature of the impedances R_1 and R_2. One might also point out that, since the temperature of the substrate varies along its length, the contribution, per unit length, to R_2 depends upon the local temperature of the substrate. A more detailed calculation, taking both of the above considerations into account was performed. The results of the lumped-impedance model were confirmed exactly to first order in $\frac{\Delta T}{T_R}$.

An alternative arrangement, in which the thermometer and heater positions were interchanged, was also used. This arrangement is shown schematically in Figure 13, below.

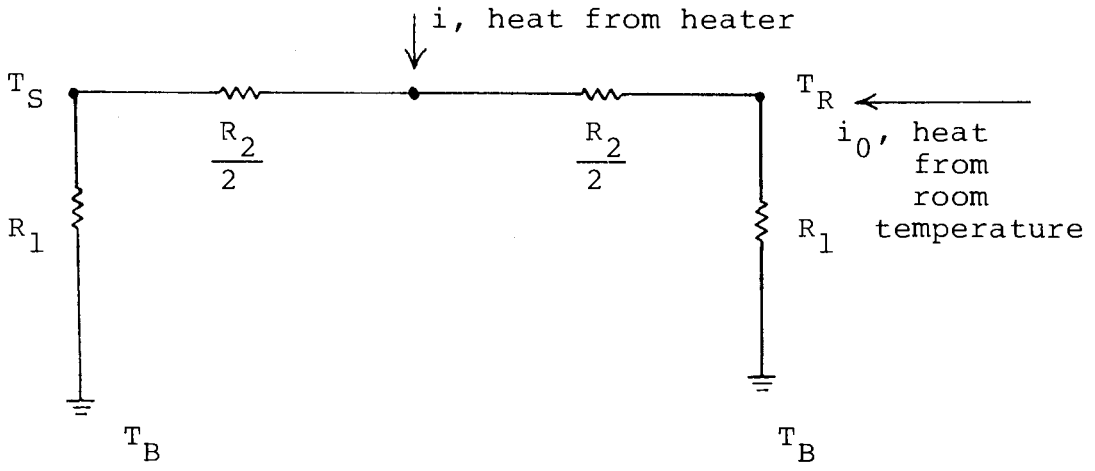

Figure 13

For this model, it is easily shown that

$$\Delta T = 2(T_R - T_B) - R_1(i_0 + i) \qquad \text{Eq 13}$$

With the additional assumption that i is linearly dependent upon T_R, we have

$$\Delta T = a + bT_R \qquad \text{Eq 14}$$

The attractive feature of this arrangement is that the temperature dependence of the substrate conductivity does not enter

into the analysis. Therefore, one does not have the above-mentioned difficulties with the inverse-T_R-dependence of the fitting function. However, thermometry was found to be less reproducible from one temperature sweep to the next than it was with the former arrangement. This is probably due to the strong dependence of ΔT upon R_1, and hence upon exchange gas pressure, with the arrangement of Figure 13.

ΔT's calculated from the above formulae were typically about .1K, or less.

SQUID SIGNAL (THEORETICAL): It is possible to calculate, from first principles, the relationship between the measured SQUID signal and the susceptibility of the sample. This theoretical calculation is given below, followed by an experimental verification.

Since the flux transformer is a superconducting loop, and therefore contains fixed flux, it is easily shown that the flux coupled into the SQUID by the secondary coil of the flux transformer is given by

$$\phi_S = \frac{M\,N}{L_P + L_S + L_L}\phi_{ext} \qquad \text{Eq 15}$$

where M is the mutual inductance between the SQUID and the secondary coil, N is the number of turns on each of the pickup loops, ϕ_{ext} is

the flux externally applied to the pickup loops, L_P is the total self-inductance of the pickup loops, L_S is the self-inductance of the secondary coil, and L_L is the inductance of the leads connecting the primary to the secondary.

In our case $L_{P+}L_S >> L_L$ (see References 27,45) so we have

$$\phi_S \simeq \frac{M N}{L_P + L_S} \phi_{ext} \qquad \text{Eq 16}$$

Since the sample dimensions are much smaller than those of the pickup loops or their separation, the sample can be approximated by a magnetic dipole of moment m. We place the dipole at the origin of a spherical polar coordinate system as shown in Figure 14.

We assume that the pickup loops have approximately equal areas, A_1 and A_2, (directed in opposing senses in each loop) and are exposed to the same applied field, H. The sample has an effective area A_{eff} and contributes flux ϕ_1 and ϕ_2 to loops 1 and 2 respectively. A_{eff} is defined so that

$$\phi_1 = A_{eff}\, 4\pi \mathcal{M} \qquad \text{Eq 17}$$

where

$$\mathcal{M} = \frac{m}{V} \qquad \text{Eq 18}$$

is the sample magnetization, and V is the sample volume.

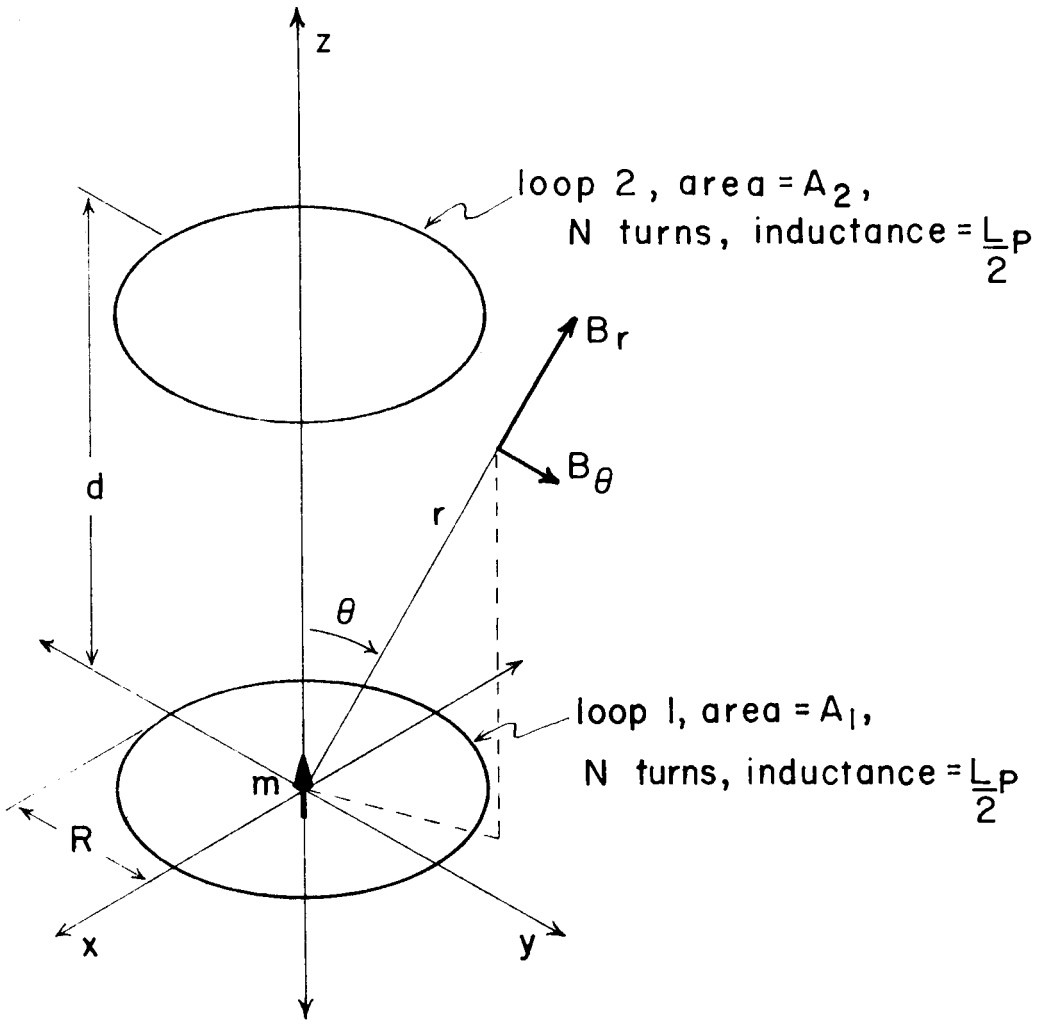

Figure 14:

Model for coupling of sample to the two pickup loops. Sample is simulated by a magnetic dipole, m, situated at the origin of a spherical polar coordinate system.

Now we can write

$$\Phi_{ext} = \Phi_1 + A_1 H - \Phi_2 - A_2 H \qquad \text{Eq 19}$$

$$A_1 \simeq A_2 \qquad \text{Eq 20}$$

We are interested in the quantities

$$\Phi_1 = \int_{loop1} \vec{B} \cdot \vec{da} \quad \text{and} \quad \Phi_2 = \int_{loop2} \vec{B} \cdot \vec{da} \qquad \text{Eq 21}$$

where $\vec{B}$ is the magnetic induction due to the dipole sample. Any good text on electromagnetic theory (see References 33,52, for example) derives expressions for B due to a dipole, but these are not analytical in the "near zone" - i.e. for r comparable to the sample dimensions. In order to avoid consequent difficulties in the calculation of Φ_1, we assume that there are no magnetic monopoles in our region of space, and write

$$\Phi_1 = -\int_{\sim loop1} \vec{B} \cdot \vec{da} \qquad \text{Eq 22}$$

where ~loop1 denotes (the infinite plane coplanar with loop 1) minus (loop 1).

Since sample dimensions are much smaller than both the radius, R, of the loops, and their separation, d, we can now use the far zone fields:

$$B_r = \frac{2\,m}{r^3}\cos\theta \qquad \text{Eq 23}$$

$$B_\theta = \frac{m}{r^3}\sin\theta \qquad \text{Eq 24}$$

Straightforward integration yields

$$\phi_1 = \frac{2\pi m}{R} \qquad \text{Eq 25}$$

$$\phi_2 = \frac{2\pi m R^2}{\left[d^2 + R^2\right]^{3/2}} \qquad \text{Eq 26}$$

For the dimensions d and R actually used (see Appendix E),

$$\frac{\phi_1}{\phi_2} = 30 \qquad \text{Eq 27}$$

Invoking the definition of A_{eff} (Eq 17), we now have

$$A_{eff} = \frac{\phi_1}{4\pi\mathcal{M}} = \frac{V}{2R} \qquad \text{Eq 28}$$

V is actually the volume in which $\mathcal{M} \neq 0$, i.e. the volume enclosed by the supercurrent shell in a superconducting sample. If the penetration depth of the superconductor is small compared to the

sample dimensions, and if demagnetization effects can be neglected, V is the sample volume. We will make these assumptions.

Using

$$\mathcal{M} = \chi H \qquad \text{Eq 29}$$

we can now write ϕ_1 in terms of sample dimensions, thus

$$\phi_1 = 4\pi\chi H \frac{V}{2R} \qquad \text{Eq 30}$$

Inserting these results into our original expression for ϕ_{ext} (Eq 19), we have

$$\phi_{ext} = \left(1 - \frac{\phi_2}{\phi_1}\right) 4\pi\chi \frac{V}{2R} H + (A_1 - A_2) H \qquad \text{Eq 31}$$

It is the second term in the above expression that can contribute extraneous signals when one varies H. As previously mentioned, attempts to null this signal by the application of a compensating field gave unsatisfactory results. Therefore all data were collected in constant field and we will consider χ to be the independent variable.

Returning to our expression for the flux coupled to the SQUID (Eq 16), we write

$$\phi_S = \frac{M N}{L_P + L_S}\left(1 - \frac{\phi_2}{\phi_1}\right) 4\pi\chi \; H \frac{V}{2R} + \text{constant} \qquad \text{Eq 32}$$

The SQUID has a built-in calibration in the form of the flux quantum, ϕ_0. By applying a known feedback signal and observing the consequent shifting of the SQUID pattern on the oscilloscope display, one can deduce the relationship between the SQUID feedback signal, V_S, and ϕ_S. For our particular SQUID the relationship is

$$V_S = 1.45 \text{ volts} \times \frac{\phi_S}{\phi_O} \qquad \text{Eq 33}$$

This calibration was checked from time to time and found to be constant to 3 significant figures.

The inductances M, L_P, and L_S were calculated from empirical formulae given in Reference 27. L_P and L_S were cross-checked using Eq 3. See Appendix E for numerical results.

We have now calculated all of the numbers needed to calibrate the measured SQUID feedback signal in terms of sample susceptibility.

$$V_S = k \; 4\pi\chi V H + \text{constant} \qquad \text{Eq 34}$$

where

$$k = 1.01 \times 10^5 \text{ volts}/(\text{gauss-cm}^3) \qquad \text{Eq 35}$$

Since we observe only the manner in which the signal varies with temperature, the constant term in Eq 34 is of no importance.

SQUID SIGNAL (EXPERIMENTAL): As a verification of the above calibration calculation, the net signal change, ΔV_S, accumulated in a traversal of the superconducting transition of some of the marker samples was recorded. This change was divided by sample volume and plotted against field coil current, i_F. If one assumes that the sample went from a complete Meissner state to a normal state of negligible susceptibility, the signal change per unit volume should, according to Eq 34, be

$$\frac{\Delta V_S}{V} = k\, H \qquad \text{Eq 36}$$

The applied field, H, will be the sum of two terms. One term will be the projection, H_A, of the ambient magnetic field along the axis of the pickup loops. The relationship between H and the current, i_F, supplied to the field coil was calculated from the Biot-Savart Law, giving

$$H = 1.05 i_F \text{ gauss/mA} + H_A \qquad \text{Eq 37}$$

Taking the upward direction in the laboratory to be positive, measurement with a Hall probe yielded -.4 gauss for H_A.

The volumes of the marker samples were obtained from their dimensions as measured with the aid of an optical microscope. These

samples were all cut in regular shapes, but the calculation of volumes from sample dimensions is only good to an accuracy of about 30%. This was checked by weighing a few samples, calculating the volumes from the known density (Reference 76), and comparing with the microscope measurement. Due to the very small masses of the marker samples (~10 micro-grams), and the care required in handling them, it was considered that to weigh every one would be of marginal benefit.

According to the foregoing theoretical calculation

$$k_{theor} = 1.01 \times 10^5 \text{ volts/(gauss-cm}^3\text{)} \qquad \text{Eq 38}$$

The plotted points were fitted to a least squares straight line and experimental values of the quantities k and H_A extracted:

$$k_{exp} = 1.16 \times 10^5 \text{ volts/(gauss-cm}^3\text{)} \qquad \text{Eq 39}$$

$$H_{Aexp} = -.4 \text{ gauss} \qquad \text{Eq 40}$$

In obtaining this fit, the optical estimates of sample volumes were adjusted within their error limits in order to get the best match of slopes between samples. See Figure 15 for a plot of the adjusted points and the least squares line.

This sensitivity is more than sufficient to observe a Meissner Effect in samples with dimensions of a fraction of a millimeter in fields of the order of 1 oersted. Prober (Reference 50) suggests

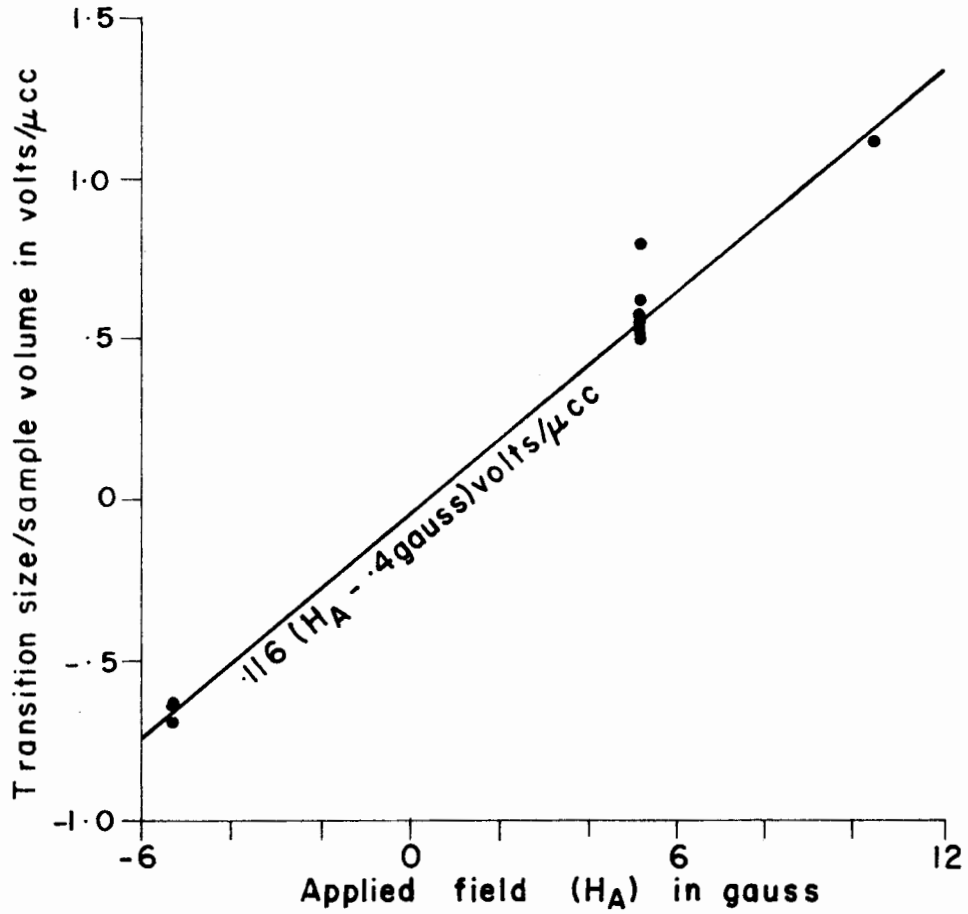

Figure 15:

SQUID signal calibration. All points are for tin samples.

that samples of intercalated TaS_2 below this size should be essentially free of the defects observed in larger samples.

The density of $TaS_2(aniline)_{3/4}$ was calculated to be 2.27 gm/cm^3 on the basis of stoichiometry and crystal structure data given in References 14,15, and 47. This was needed for the purpose of deriving the volumes, V, of the small irregularly-shaped samples from their measured weights. Results were in order-of-magnitude agreement with estimations of sample volumes made by measuring their dimensions with a microscope.

The digitized SQUID signal was processed by first subtracting contributions due to the marker samples. Next, the arbitrary constant was removed by setting the normal-state signal equal to zero. Finally, the results of the above calibration were applied to calculate χ from V_S.

EXPERIMENTAL RESULTS AND CONCLUSIONS

A few of the $TaS_2(aniline)_{3/4}$ susceptibility plots are shown in Figures 16 and 17. All measurements were performed while warming the samples in fields of 1-30 gauss, applied parallel to the layers. The most striking feature of these transitions is their extraordinarily small size. It was consistently the case that the transition amplitude was less than 20% of that which would be expected for a sample which had been warmed from a fully diamagnetic state. A tin transition observed under the same conditions is shown in Figure 18 for comparison.

Samples 16 and 21 (see TableII) displayed no transition at all between 1.6K and 4.2K, despite the fact that these samples were large enough that a transition, if it occured, ought to be resolvable.

FLUX PINNING: The $TaS_2(aniline)_{3/4}$ samples displayed no detectable Meissner Effect upon cooling, indicating the presence of a large number of flux pinning sites. Pinning was also observed in the Tl samples, but not in Sn or In, which usually displayed completely reversible transitions upon thermal cycling. This is probably due to the relatively low melting points of Sn and In, which allows them to anneal at room temperature, thereby removing pinning sites.

Since the samples were cooled, not in zero field, but in some

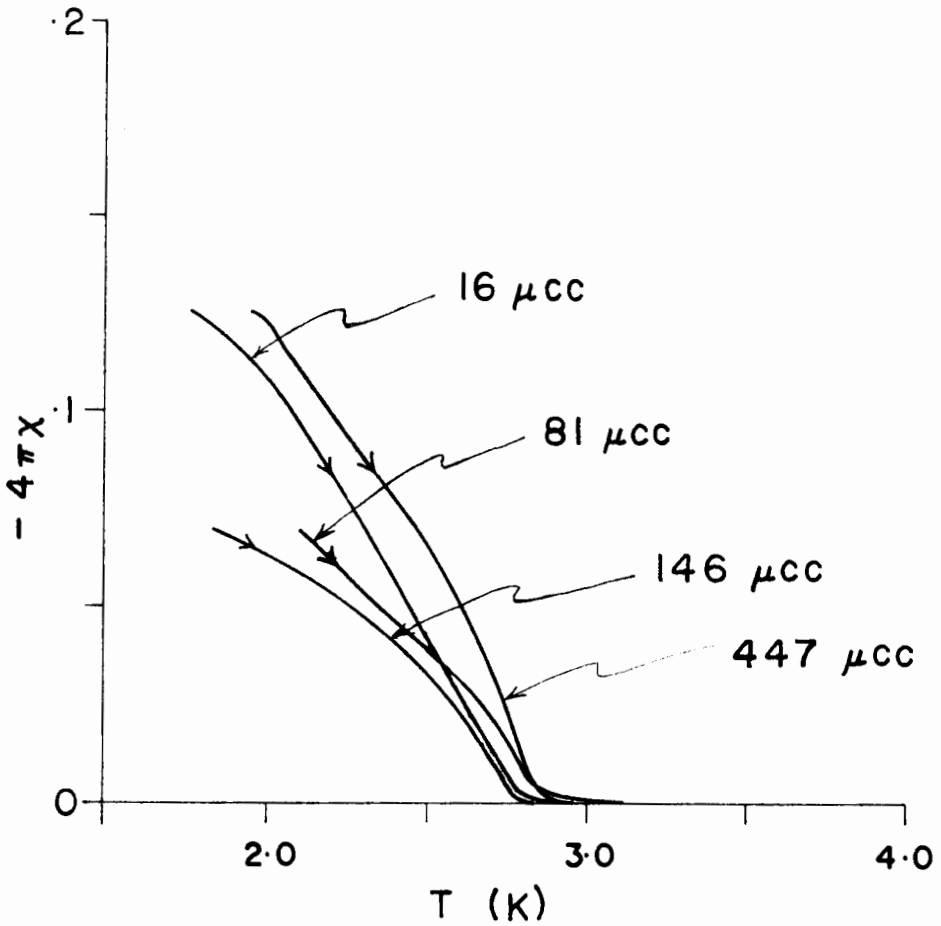

Figure 16:

Transitions of $TaS_2(aniline)_{3/4}$ samples of various sizes. All curves were taken in a field of 5.25 gauss applied parallel to the layers. Note vertical scale.

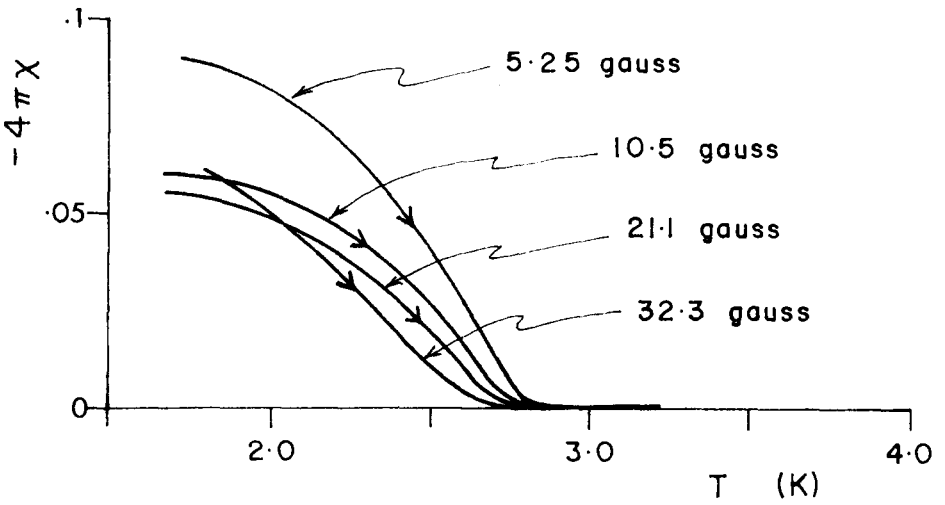

Figure 17:

Superconducting transitions of $TaS_2(aniline)_{3/4}$ sample #19 in various fields applied parallel to the layers. Note vertical scale.

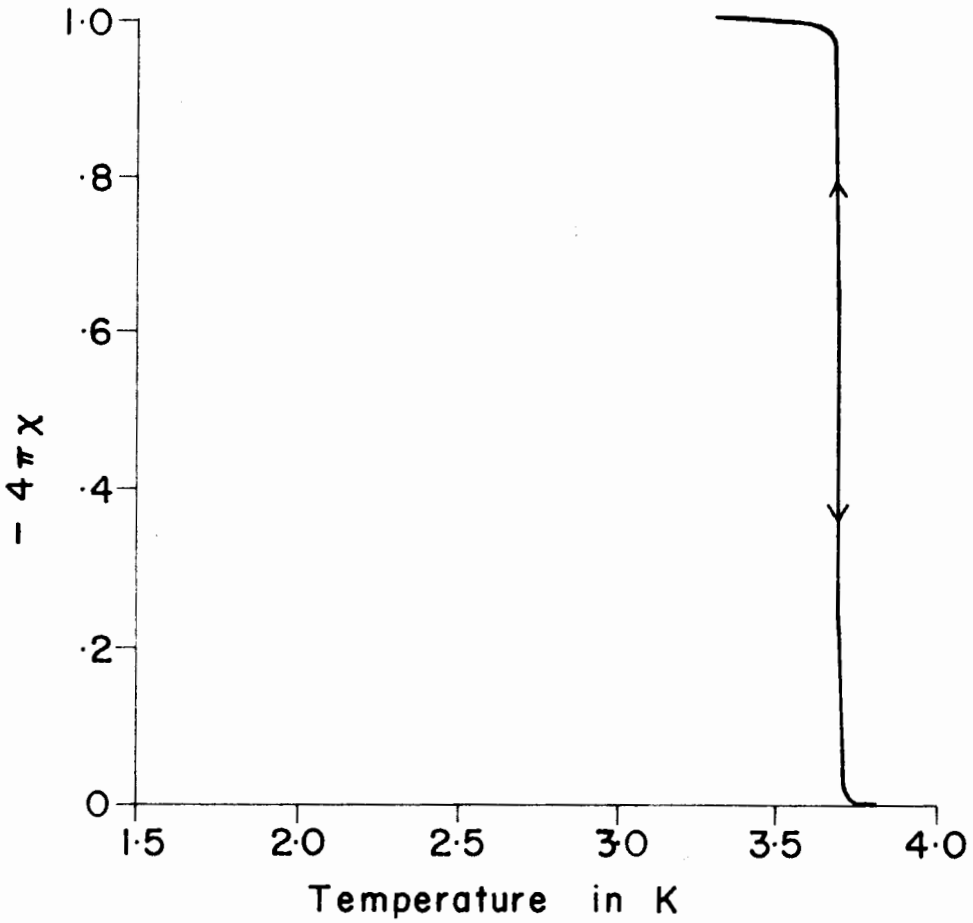

Figure 18:

Superconducting transition of tin in a field of 5.25 gauss. Sample is a thin platelet with volume of about 10^{-5} cc. Field was applied parallel to the plane of the sample. Compare with Figures 16 and 17.

finite remnant field (~.5 gauss, cf Eq 37), flux pinning effects create some ambiguity as to the size of the effective applied field. For this reason, only Sn and In samples were used in the SQUID signal calibration. However, since the ambient field represents only 10%, or less, of the applied field, this same ambiguity could not explain the very small size of the $TaS_2(aniline)_{3/4}$ transitions.

The absence of a Meissner Effect upon cooling is confirmed by measurements of Gamble et al (Reference 22) upon $TaS_2(pyridine)_{1/2}$. Prober reports (Reference 50) a small expulsion of flux upon cooling this material with field applied parallel to the layers. However, he claims that the signal measured is larger by several orders of magnitude than that which would be expected for a series of isolated TaS_2 sandwiches. This, together with the specific heat data of Gamble et al (Reference 24), seems to indicate that superconductivity in intercalated layer compounds is indeed a bulk effect.

TRANSITION WIDTHS: Reported transition widths are not incompatible with the present data. Prober (Reference 50) concludes that the broad transition is not due to passage through the mixed state or to demagnetization effects, but may be caused by the presence of regions in the sample which are only partially intercalated, or are slightly misaligned with respect to the rest of

the layers. Both of these interpretations seem reasonable in the light of the present results, as will be shown below.

TRANSITION AMPLITUDES: There is considerable error in the measurement of sample volumes, especially for the marker samples. However, this could not explain the very small observed transition amplitudes.

One might assume that the samples were not fully intercalated, or contained excess aniline. To check this, one sample was heated in an argon atmosphere at ~200C for about 18 hours in order to drive out the intercalate. The weight loss was 17% of the original sample weight, indicating that the sample had been 78% intercalated before heating. Further heating for several days at 150C failed to produce any additional weight loss. Another sample was soaked in ethanol for 24 hours. This should dissolve any excess aniline, or any aniline which is only loosely bound to the TaS_2. The sample weight was not affected by this procedure. The transition amplitude was 10% larger after soaking, but otherwise unchanged. It was felt that this difference was within experimental error.

As a further check on the signal calibration procedure, separate calibrations were performed for each $TaS_2(aniline)_{3/4}$ transition, by normalizing the signal to the size of the marker sample transitions observed in the same temperature sweep. No significant

change in transition size was effected.

One might argue that the demagnetization factors of the samples could account for a smaller signal than expected, since no demagnetization effects were assumed in the signal calculation. If this were so, one would expect to see a correlation between sample size and transition size. No such correlation was observed. Besides, the shapes of the $TaS_2(aniline)_{3/4}$ samples were not different enough from the shapes of the marker samples to account for a tremendous disparity in demagnetization factors.

In order to determine whether or not our samples ever entered a fully diamagnetic state, we will use data from the literature to make an estimate of H_{C1}. We will also calculate the penetration depths, $\lambda_{//}$ and $\lambda_{\perp}$, in order to decide to what extent flux penetration might decrease the diamagnetic response of such small samples.

CALCULATION A: One theoretical model which has met with considerable success in application to anisotropic superconductors is constructed by using an effective-mass tensor in the Ginzburg-Landau equations. Treatment of the theory and comparison with experiment can be found in References 20,36,44,46,50. We will assume that $TaS_2(aniline)_{3/4}$ can be characterized by such a model.

We start with the conventional definitions of the Ginzburg-

Landau parameters, κ_1 and κ_3,

$$\kappa_1 = \frac{H_{C2}}{\sqrt{2}\, H_C} \qquad \text{Eq 41}$$

$$H_{C1} \simeq \frac{H_C \ln \kappa_3}{\sqrt{2}\ \kappa_3} \quad \text{for } \kappa >> 1 \qquad \text{Eq 42}$$

Close to the zero-field transition temperature, T_C,

$$\kappa_1 \simeq \kappa_3 \simeq \kappa \qquad \text{Eq 43}$$

so we have

$$H_{C1} \simeq \frac{H_C^2}{H_{C2}} \ln\left(\frac{H_{C2}}{\sqrt{2}\, H_C}\right) \qquad \text{Eq 44}$$

The critical fields display the usual linear temperature dependence for T close to T_C. Therefore,

$$H_{C1} \simeq H_C \frac{H_C'}{H_{C2}'} \ln\left(\frac{H_{C2}'}{\sqrt{2}\, H_C'}\right) \qquad \text{Eq 45}$$

where the prime denotes a derivative with respect to temperature near T_C.

From Eq 12, for T close to T_C,

$$H_C \simeq - T_C H_C' \left(1 - \frac{T}{T_c}\right) \qquad \text{Eq 46}$$

where

$$H_C' = - \frac{2 H_0}{T_c} \qquad \text{Eq 47}$$

This allows us to write

$$H_{C1} \simeq -\left(1 - \frac{T}{T_c}\right) \frac{4 H_0^2}{T_c H_{c2}'} \ln\left(\frac{- T_C H_{C2}'}{2\sqrt{2}\ H_0}\right) \qquad T \simeq T_C \qquad \text{Eq 48}$$

H_0 can be found from the specific heat discontinuity, ΔC, at T_C. Accordingly,

$$H_0 = 100\text{-}180 \text{ gauss}, \qquad \text{Eq 49}$$

depending upon how one interprets the data of Reference 16.

Quoting Prober's results (Reference 50) for $TaS_2(\text{aniline})_{3/4}$,

$$H_{C2//}' \equiv \frac{dH_{C2//}}{dT} = - (50\text{-}96) \text{kG/K} \qquad \text{Eq 50}$$

In summary, taking $T_C = 2.9$K, we calculate $H_{C1//} \simeq .5\text{-}3$ gauss at T = 1.5K. This estimate for the lower critical field parallel to the layers indicates that our samples may have entered (or, at least, almost reached) a fully diamagnetic state at the temperatures and

fields which were obtained in the Sample Chamber.

Resuming our calculations, Eq 41 immediately gives us

$$\kappa_{//} = \frac{- H'_{C2//} T_C}{2\sqrt{2}\ H_0} \qquad \text{Eq 51}$$

Since

$$\kappa_{\perp} = \sqrt{\frac{m}{M}}\ \kappa_{//} \qquad \text{Eq 52}$$

we also extract the effective mass ratio, m/M, from Prober's data, allowing calculation of the anisotropic Ginzburg-Landau parameters near T_C.

Lawrence and Doniach (Reference 44) give us

$$H'_{C2//} = \frac{- \phi_0}{2\pi \xi_{//}^2 T_C \sqrt{\frac{M}{m}}} \qquad \text{Eq 53}$$

and

$$\xi_{\perp} = \sqrt{\frac{m}{M}}\ \xi_{//} \qquad \text{Eq 54}$$

from which we can calculate the superconducting coherence lengths, $\xi_{\perp}$ and $\xi_{//}$. The corresponding penetration depths come from

$$\kappa_{\perp} = \frac{\lambda_{//}}{\xi_{//}} \qquad \text{Eq 55}$$

and

$$\kappa_{//} = \left(\frac{\lambda_{\perp} \lambda_{//}}{\xi_{\perp} \xi_{//}} \right)^{1/2} \qquad \text{Eq 56}$$

CALCULATION B: As a cross-check on the results of the above calculations, we will also make rough estimates of some of the above quantities using the Ginzburg-Landau approximations for an isotropic superconductor. We use the expressions obtained for the limit in which the mean free path is much shorter than the BCS coherence length (i.e. $l \ll \xi_0$). We believe this "dirty" limit to be appropriate in $TaS_2(\text{aniline})_{3/4}$ due to the overwhelming evidence of light-scattering measurements (Reference 50), the present observations of flux pinning, and the visually obvious imperfection of the crystals. Accordingly, from Werthamer (Reference 66), we have

$$\lambda_d = .61 \ \lambda_L \sqrt{\frac{\xi_0}{l}} \qquad \text{Eq 57}$$

$$\xi_d = .86 \sqrt{\xi_0 l} \qquad \text{Eq 58}$$

$$\kappa_d = .72 \sqrt{\frac{\lambda_L}{l}} \qquad \text{Eq 59}$$

for the dirty limit results, where λ_L is the London penetration depth;

$$\lambda_L = \left(\frac{mc^2}{4\pi ne^2}\right)^{1/2} \qquad \text{Eq 60}$$

and ξ_0 is the BCS coherence length;

$$\xi_0 = .18\,\frac{\hbar\, v_F}{k\, T_c} \qquad \text{Eq 61}$$

For a simple free-electron gas model, we can calculate the electron density, n, the Fermi velocity, v_F, and the mean free path, l, in terms of the electrical resistivity, ρ, of the material and its electronic heat capacity, γT. Re-writing Eqs 57,58,59 in terms of these experimentally measurable quantities,

$$\lambda_d = 6.4\times10^{-3}\left(\frac{\rho}{T_c}\right)^{1/2} \quad \text{cm} \qquad \text{Eq 62}$$

$$\xi_d = 8.6\times10^{-7}\left(\frac{1}{\rho\gamma T_c}\right)^{1/2} \quad \text{cm} \qquad \text{Eq 63}$$

$$\kappa_d = 7.5\times10^{3}\left(\rho\gamma\right)^{1/2} \qquad \text{Eq 64}$$

where ρ is in ohm-cm and γ is in $\text{erg/cm}^{-3}\text{K}^{-2}$.

γ is obtained from Reference 16, but it appears that the resistivity of $TaS_2(\text{aniline})_{3/4}$ has not been published. However, since this is only an order-of-magnitude calculation, we can use the published (Reference 59) resistivities of the structurally-similar material, $TaS_2(\text{pyridine})_{1/2}$:

$$\rho_{\perp} = 6 \text{ ohm-cm} \qquad \text{Eq 65}$$

$$\rho_{//} = 6\text{x}10^{-5} \text{ ohm-cm} \qquad \text{Eq 66}$$

for conduction perpendicular to the layers, and parallel to the layers, respectively, at 4K.

Since $\kappa_{\perp}$ involves electron motion parallel to the layers, clearly we have

$$\kappa_{\perp} = 7.5\text{x}10^{3}\ \rho_{//}\ \gamma^{1/2} \simeq 12 - 17 \qquad \text{Eq 67}$$

The situation is not so transparent for $\kappa_{//}$, but, by comparison with Eq 56, we flatly state that a reasonable expression would be

$$\kappa_{//} = 7.5\text{x}10^{3}\ (\rho_{//}\rho_{\perp})^{1/2}\ \gamma^{1/2} \qquad \text{Eq 68}$$
$$= 3700 - 5300$$

Similarly,

$$\lambda_{\perp} = 6.4\text{x}10^{-3} \left(\frac{\rho_{\perp}}{T_c}\right)^{1/2} \qquad \text{Eq 69}$$

$$\xi_{\perp} = 8.6\text{x}10^{-7} \left(\frac{1}{\rho_{\perp}\gamma\ T_c}\right)^{1/2} \qquad \text{Eq 70}$$

with analogous equations for λ and ξ in the parallel direction.

Results of both of the above sets of calculations are given in the following table for comparison.

Experimentally measured quantities:

Calculation A	Calculation B	References
crystal structure	crystal structure	14,15,47
ΔC=16-49 mJ/mole/K		16
T_c = 2·87 - 3·0K	T_c = 2·87-3·0K	16,50,present work
$\sqrt{M/m}$ = 25-37		50
$-H'_{C2//}$= 50-96 kG/K		50
	γ = 9·5 - 19 mJ/mole/K^2	16
	$\rho_\perp$ = 6 ohm-cm	59
	$\rho_{//}$ = 6 × 10^{-5}ohm-cm	59

Calculated quantities:

Calculation A	Calculation B
mass density = 2·27 gm/cc	
unit cell volume = 230 Å^3	
1 mJ/mole = 71·9 erg/cc	
H = 100-180 G	
$-H'_{C1//}$ = ·3-2 G/K	
$\kappa_{//}$ = 280-1000	$\kappa_{//}$ = 4000-5000
$\kappa_\perp$ = 7·6-28	$\kappa_\perp$ = 10-20
$\lambda_{//}$=2200-5600 Å	$\lambda_{//}$ = 3000 Å
$\lambda_\perp$=·007-·02mm	$\lambda_\perp$ = ·09 mm
$\xi_{//}$ = 210-290 Å	$\xi_{//}$ = 200-400 Å
$\xi_\perp$ = 5·7-9·1 Å	$\xi_\perp$ = ·6-1 Å

Table IV

Sample thicknesses ranged from .02 mm to .3 mm. This range overlaps with the calculated values of $\lambda_{\perp}$, indicating that partial penetration of the applied fields into the sample could explain some of the small transitions. However, some other explanation must be sought for the larger samples.

The above calculations fail to completely rule out the possibility that the temperature sweeps did not start at low enough values of temperature and applied field to access the region below H_{C1}. This explanation is also favoured by the absence of any "foot" at the low temperature end of the transition curves. Such a foot would indicate a traversal of H_{C1}. It would be necessary to use a vacuum pump of larger capacity than that which was available to reach lower temperatures. Lower fields could be obtained by the application of a small field to cancel the vertical component of the ambient field in the cooling portion of the temperature sweep cycle. Alternatively, a set of Helmholtz coils could be used to create a field-free region in the Sample Chamber. This "zero field" would be frozen in by the superconducting shield surrounding the lower portion of the cryostat during the initial helium transfer.

The most reproducible feature of our data is the point of sharpest curvature in the susceptibility vs temperature curves. This has also been noticed by other authors (References 24,51) in AC and DC measurements upon layer compounds. Figure 19 illustrates the

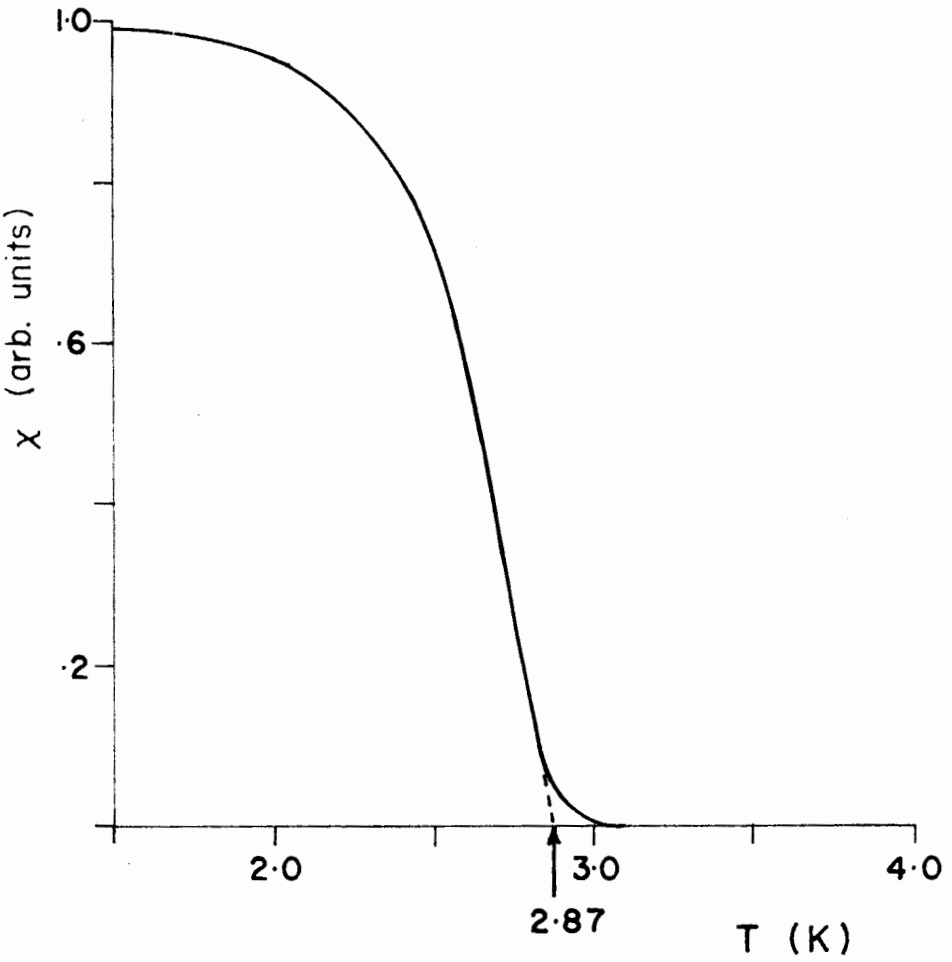

Figure 19:

Superconducting transition of $TaS_2(aniline)_{3/4}$ taken from the AC susceptibility data of Reference 16. The arrow indicates our definition of T_c.

relationship between this temperature and our definition of T_C. The plot of $H_{C2//}$ vs T_C given in Figure 20 was obtained using our definition of T_C. This plot gives 2.87-2.89K for the zero-field transition temperature. This is to be compared with 2.87K obtained from the data of DiSalvo et al (Reference 16) shown in Figure 19. The slope of $H_{C2//}$ vs T obtained by any reasonable fit to the points in Figure 20 is less than 250 G/K. This value is much less than that obtained by Prober. (See table on p73.) Due to the large anisotropy of $TaS_2(aniline)_{3/4}$, a slight misalignment of the crystal can produce large changes in the upper critical field. A simple calculation using the angular dependence of H_{C2} as derived by Lawrence and Doniach in Reference 44;

$$H_{C2}(\theta,T) = \frac{\Phi_0}{2\pi\xi_{//}^2(T)} \left[\sin^2\theta + \frac{m}{M}\cos^2\theta\right]^{-1/2} \qquad \text{Eq 71}$$

(θ = angle between layers and applied field)

shows that a 1-degree misalignment of the sample with respect to the applied field would depress $H_{C2//}$ by about 10%. A 2-degree misalignment would cause a depression of 25% to 40%, depending upon which value of the effective mass ratio one takes from Reference 50. Since little care was taken to properly align the crystals, these figures are probably indicative of the error in our measurement of $H_{C2//}$. Calculations such as these could account for some of the

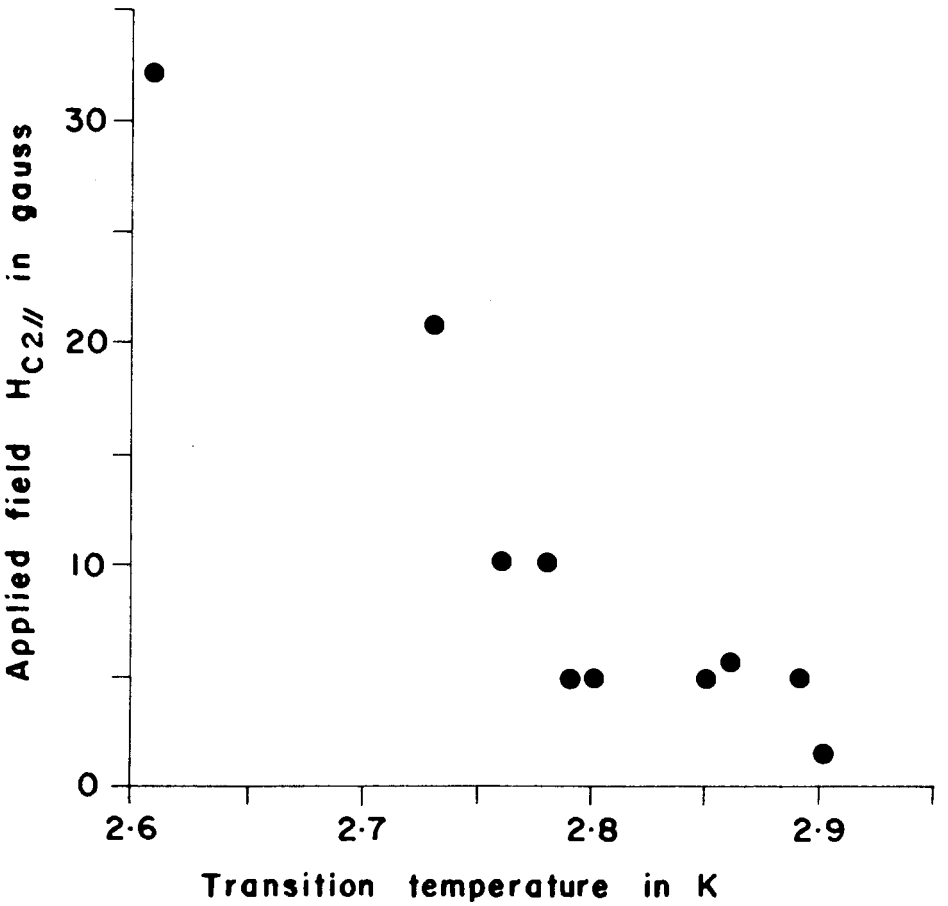

Figure 20:

Observed transition temperatures of $TaS_2(aniline)_{3/4}$ samples with field applied parallel to the layers.

discrepancy between Prober's data and the results shown in Figure 20.

There were occasional indications of a positive contribution to the susceptibility. Such results were not reproducible and were most probably caused by solid air, which tends to accumulate in the bottom of the Sample Chamber. There was no indication of the large paramagnetic effect reported by DiSalvo in Reference 14.

In summary, a sensitive magnetometer has been built, and shown to operate according to theoretical predictions. It has also been demonstrated that none of the $TaS_2(aniline)_{3/4}$ samples tested displayed perfect diamagnetism under the experimental conditions imposed. Calculations of the lower critical field parallel to the layers are not inconsistent with this observation. The complete absence of a transition in some of the smaller samples lends support to the hypothesis that much of the observed behaviour of intercalated layer compounds is governed by the presence of crystal imperfections which have a characteristic length, in $TaS_2(aniline)_{3/4}$, of about .1 mm.

SUGGESTIONS FOR FURTHER WORK

The SQUID resolution is ultimately limited by thermal noise (see Reference 27), and our SQUID system falls short of this limit by a factor of about 100. Correspondingly smaller samples in lower fields could be observed, if the system's electronics were improved so as to reduce 60Hz noise.

A further factor of 100 is lost due to the poor coupling between the SQUID and the sample. As can be seen from Figure 2 (p8), this coupling could be improved by reducing the size of the pickup loops, but only at the expense of the ability to change samples quickly.

One might suggest that the signal seen for a given sample size might be amplified merely by increasing the applied field. There are several reasons why this was not done. The most serious resulting difficulty would be an increased level of vibrationally induced noise. At higher fields, field gradients are generally larger, and so is the signal generated by a given amplitude of motion in that field. This effect was easily observed in going from a field of 5 gauss to 20 gauss. It was also noticed that, at fields of about 30 gauss, the SQUID often required re-tuning, due to the effect of the field upon the critical current of the SQUID's point contact. Therefore the SQUID would have to be better shielded from the field coil at higher fields.

Aside from the above-mentioned points relating to high field measurements there are two other factors to be considered when observing transitions of type II superconductors. The width of such a transition is determined by the difference between H_{C1} and H_{C2}, which is larger for higher fields. This means that it becomes progressively more difficult to capture the whole transition as the field is increased. This may be especially important in the case of $TaS_2(aniline)_{3/4}$, where the data seem to indicate the possibility of a very low H_{C1}. Moreover, since the magnetization of a type II superconductor is maximum for an applied field $H = H_{C1}$, the observed signal will actually be smaller for applied fields greater than this limiting value.

However, there is a way that one might be able to "have his cake and eat it too". This would involve a second flux transformer mounted so as to improve the coupling between the samples and the existing pickup loop. The calculations in Appendix H show that coupling to the sample could be improved by a factor of 30 in this manner.

Thermometry might be improved by grinding the thermometer to remove its insulating coating. This would permit better thermal contact between the thermometer and the substrate, making possible a better approximation to the true sample temperature. However, the

thermometer would, of course, have to be re-calibrated if this were done.

In future, all superconducting materials and solders should be avoided in construction of this type of cryostat.

In summary, by cooling small $TaS_2(aniline)_{3/4}$ crystals to lower temperatures in lower, well-aligned fields, one may be able to establish the intrinsic properties of this material. If necessary, the magnetometer sensitivity could be increased, as outlined in Appendix H.

APPENDIX A

FEEDTHROUGHS: A selection of home-made and commercial vacuum feedthroughs were leak-tested at both room temperature and liquid nitrogen temperature. The aim was to find a feedthrough which would be suitable for cryogenic applications.

The commercial feedthroughs all involved some sort of glass-to-metal seal. None was found to be consistently reliable. It was assumed that the differential thermal contraction of the glass and the metal caused these seals to fail.

The home-made feedthroughs consisted of a metal tubing which was soldered into a metal vacuum bulkhead. The wire(s) were then run through the tubing and sealed with epoxy at the open end of the tube. The epoxy was always applied so as to form a blob enclosing the end of the tube. This latter measure was taken in hopes that the epoxy would tighten around the metal as it cooled, thereby ensuring a good seal at all temperatures.

The tubings used were cupronickel (outer diameter = 1.2 mm; wall thickness = .3 mm) and softened copper capillary tubing (outer diameter = 2.9 mm; inner diameter = .6 mm). The copper tubing was softened by heating it red hot and then quenching it.

The epoxies used were Stycast 2850 FT, with 24LV catalyst, and Stycast 1266. (See Note 3.)

The wires used were tightly twisted pairs of niobium or T48B. (See Notes 1 and 2.)

None of the home-made feedthroughs failed.

APPENDIX B

LIQUID NITROGEN CONTROLLER: The automatic level controller for the liquid nitrogen was a source of continual annoyance. If this device is faulty, it can - and did - cause accidents of catastrophic proportions. For this reason, it seems worthwhile to mention some of the problems encountered and how they were solved.

The liquid level sensor consists simply of a semiconductor diode junction which conducts when it is above the liquid and has a large resistance when immersed. The sensors are Sylvania 1N126 diodes, selected by hand for desirable forward resistance versus temperature characteristics. A schematic of the electronics is shown in Figure 21. This aspect of the controller was quite reliable and operated most satisfactorily. The problems lay rather with the more mechanical aspects.

The simplest problem encountered was solved merely by taking care to rigidly fix the sensor. Turbulence produced by the incoming liquid stream had gradually moved the sensor higher until it reached a height which the liquid never attained. Consequently the nitrogen continued to pour into the dewar and overflowed. Eventually, the glass dewar shattered from the stresses imposed by contraction of the metal collar by means of which it was mounted.

The solenoid valve can be used to switch the flow of liquid from

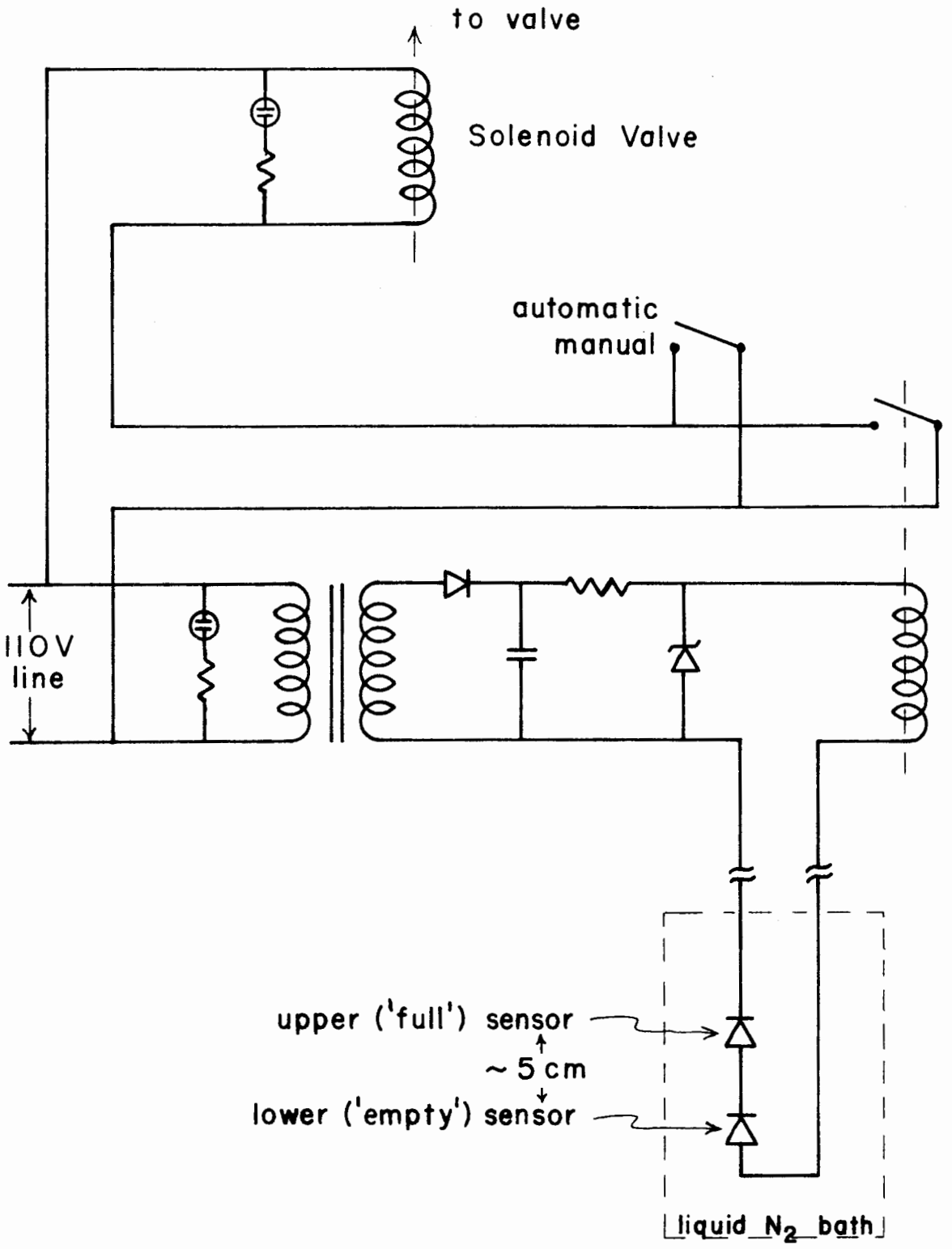

Figure 21: Liquid nitrogen level controller.

a pressurized storage dewar, or alternatively, to switch the flow of gas which pressurizes the storage dewar, thereby initiating the transfer. The former approach resulted in erratic behaviour of the valve due to the large temperature range through which it was required to operate. There also seem to be difficulties associated with the storage of the liquid under pressure: The sudden reduction of the vapour pressure of the liquid nitrogen upon transfer seems to cause thermal and mechanical turbulence in the liquid, resulting in spurious triggering of the level sensor. For these reasons it was found to be much more satisfactory to control the transfer of liquid by switching the pressurizing gas. It was necessary to use an SPDT solenoid valve for this application so that the pressure in the storage dewar was relieved after each transfer.

Spurious triggering of the sensor can also be caused by a poorly designed opening on the cryostat end of the liquid nitrogen transfer tube. Turbulence at this point was damped by affixing a gauze nozzle made from braided copper ground strapping and glass wool.

One other possible eventuality is that the storage dewar runs out of liquid. In itself, this is not very serious, as the nitrogen remaining in the cryostat will still last for some time. However, the controller will continue to supply pressurizing gas in this circumstance, which results in warming of both the cryostat and the storage dewar and in the consumption of a large quantity of gas. It

was therefore found preferable to supply the pressurizing gas from a small reservoir. The boiloff from a second storage dewar was ideal for this purpose.

It was also necessary to mount the electronics at a location several feet away from the cryostat in order to prevent the switching pulses of the controller from disturbing the SQUID.

With the above modifications, the level controller operated with great reliability, besides being very efficient in the consumption of liquid nitrogen.

APPENDIX C

EPOXY CURING RECIPE: Since epoxy is extensively used in cryogenic systems, properties and curing techniques are worth mentioning. The particular type of epoxy referred to throughout most of this work is Emerson and Cuming Stycast 1266. (See Note 3.) This epoxy consists of two liquid components which are mixed in a 100:28 ratio by weight. The mixture is of very low viscosity, cures at room temperature, and can readily be cast in a mold of virtually any size or shape. However, since 1266 cures by means of an exothermic reaction and is also a good thermal insulator, batches larger than about 50cc (depending upon geometry) can suffer from overheating in the curing process. Effects of this overheating include tremendously shortened curing time (as short as 5 minutes), discoloration, warping, and formation of gas pockets in the epoxy. With a little experimenting it was found that the following recipe yielded a finished product which was not only free of all of the above defects, but was far superior in appearance to anything produced by any other methods attempted:

1) Mix thoroughly for 2 to 3 minutes 200 grams part A with 56 grams part B. Pour into a mold of desired shape.

2) Pump on the mixture with a mechanical vacuum pump for about 5 minutes, to eliminate dissolved air, water, or solvents. It may be

necessary to regulate pumping speed in order to prevent the epoxy from boiling over the edges of the container. A cold trap can be used to protect the pump from harmful vapours.

3) Place in freezer compartment of an ordinary household refrigerator for about one half hour.

4) Allow to cure in the main refrigerator compartment (~5C) for about 18 hours.

5) Allow to cure at room temperature for about 5 hours.

With adjustments of the various time periods involved, this same recipe could be applied to batches of different sizes or shapes. However, batches larger than the above 256 grams become unwieldy in that the epoxy begins to overheat in the 2 to 3 minutes it takes to mix it.

The above recipe was developed for curing batches with the maximum volume to surface area ratio - i.e. the geometry for which the overheating problem is most serious. For different mold shapes the time periods can be shortened.

Containers made of almost any non-porous material with a sufficiently slippery surface can be used successfully for molding 1266. Both Nalgene and Pyrex beakers were used successfully. Teflon and cellophane sheets also worked well.

The cured epoxy is transparent with a slight greenish tint. It has no gas pockets and is quite resistant to both mechanical and

thermal shocks. One 256 gram block survived both plunging into liquid nitrogen and falling from a height of 3 meters onto a concrete floor, and suffered no damage other than a slight dent.

Cured 1266 can be cut and machined quite easily, but will soften when heated. (In fact, a soldering iron is a useful tool for working epoxy once it has cured.) If the machining is carefully done, thicknesses down to .25-.35 mm (10-15 mils) can readily be obtained. However, as previously noted, such thin walls are quite permeable to helium at room temperature. The low thermal conductivity of the material is an asset for use in cryogenics. Its one major failing is its high coefficient of thermal expansion which makes the design of vacuum seals and feedthroughs quite elaborate.

APPENDIX D

CRYOSTAT OPERATING PROCEDURES:

1) Pump out all chambers and vacuum lines. Check for leaks. Even small leaks can cause annoying problems, such as variable thermal links, etc. Also check for and reduce He background due to desorption of He from the glass and epoxy walls of the dewar and cryostat.

2) Admit 100 microns of air to vacuum jacket separating the nitrogen and helium baths, and seal it. Admit 1 atm of nitrogen gas to Helium Bath Chamber and seal it. Evacuate Sample Chamber and Exchange Gas Chamber and seal them.

3) Fill liquid nitrogen bath and switch on liquid nitrogen controller. Allow several hours for cryostat to cool to 77K. For the purpose of deciding when thermal equilibrium is reached, one can monitor the carbon resistance thermometer in the Sample Chamber or the exchange gas pressure in the Helium Bath Chamber.

4) Switch on all electronics to allow for warm-up.

5) Pump out everything but vacuum jacket and check for leaks again.

6) Admit 100-1000 microns of pure He exchange gas to Sample Chamber and Exchange Gas Chamber and seal them. Admit slightly over 1 atm of He gas into Helium Bath Chamber. Insert transfer tube and

transfer enough liquid He to immerse the SQUID. Check to see that SQUID and other superconducting circuits are operating. Fill Bath with liquid He.

7) Remove transfer tube and wait about 15 minutes for thermal equilibrium.

8) Slowly pump Helium Bath to operating temperature.

9) Maintain Sample Chamber pressure below .01 micron and Exchange Gas Chamber pressure between .01 and .1 micron throughout the remainder of the experiment.

Once the Helium Bath is at operating temperature and the SQUID is tuned, the temperature sweep cycle is as follows.

1) Switch on field current supply and adjust to desired field.

2) Turn on heat switch to admit current to field coil.

3) Wait until SQUID has stabilized and slowly turn heat switch off.

4) Switch off field current supply.

5) Adjust SQUID for maximum stability.

6) Lower pen on X-Y recorder and slowly increase heater current taking about one minute to warm sample to 4K.

7) Raise pen, turn heat switch on, turn heater off.

8) Cool sample in zero field, and repeat cycle if desired.

Sample changing was accomplished as follows:

1) Pump on Exchange Gas Chamber until temperature in Sample Chamber rises above about 5K (1 kilohm on thermometer).

2) Admit pure He gas to Sample Chamber and maintain pressure above 1 atm to help prevent air from entering Sample Chamber.

3) Remove Sample Holder and plug Sample Chamber.

4) Wait for Sample Holder to warm sufficiently to cause any moisture which has condensed on it to evaporate.

5) Change samples and re-insert Sample Holder into Sample Chamber.

6) Pump on Sample Chamber.

7) Admit about 100 microns of pure He gas to Exchange Gas Chamber and allow Sample Chamber to cool.

8) Once proper operating pressures and temperatures are obtained, temperature sweep cycle may be started.

When a second Sample Holder was used the above changeover could be completed in 15 minutes. Six or more sample changes can be performed on one charge of liquid helium (3l at 1.6K).

APPENDIX E

APPARATUS SPECIFICATIONS:

Cryostat

Time to precool from room temperature to 77K: approx. 4 hr

Cycling time of automatic liquid nitrogen fill control: approx. 2 hr

Pressure of nitrogen exchange gas in Helium Bath Chamber at 77K: 350 mm Hg

Liquid helium charge: 5 l

Helium boiloff at 4.2K: 6 l gas (at room temperature and pressure) per minute

Net heat leak into Helium Bath at 4.2K: .3 watts

Net heat leak into Sample Chamber: 10-20 mW

Time to pump bath to 1.6K: approx. 1 hr

Time required for sample changing: 15 min

Maximum running time: approx. 12 hr

Liquid nitrogen consumption: approx. 20 l per day

SQUID

Audio frequency: 1-10 kHz

Radio frequency: 22 MHz

Full scale tracking range: 14 flux quanta (20 volts)

Detector output vs signal in pickup loop: 1.45 V/flux quantum

Peak to peak noise level at detector output in lock mode: .5 flux quantum (.7 volts) at 60Hz, .03 flux quantum (.04 volts) at SQUID audio freq.

Limit of resolution (smallest resolvable transition): 10 flux quanta sample flux (.2 volts SQUID signal)

Flux Transformer

Primary (pickup loops)

Type of wire: niobium (See Note 2.)

Wire diameter including insulation: .076 mm (4 mils)

Number of turns each coil: 6 (1 layer)

Length of each coil: .06 cm

Coil separation: 1.59 cm (5/8 inch)

Mean coil diameter: 1.10 cm

Room temperature resistance of both coils plus leads: 34 ohms

Inductance of both coils: 2 micro-henry

Mutual inductance of coils: .01 micro-henry

Secondary (in SQUID)

Type of wire: niobium (See Note 2.)

Wire diameter including insulation: .076 mm (4 mils)

Number of turns: 92 (1 layer)

Coil length: .94 cm

Mean coil diameter: .18 cm

Coil resistance at room temperature: 26 ohms

Coil inductance: 2 micro-henry

Mutual inductance to SQUID: 11 nano-henry

Main Field Coil

Type of wire: T48B (See Note 1.)

Wire diameter including insulation: .11 mm (4.3 mils)

Number of turns: 5430 (10 layers)

Coil length: 6.35 cm

Mean coil diameter: 1.38 cm

Coil resistance at room temperature: 2.1 kilohm

Coil inductance: .08 henry

Coaxial field on axis of coil at positions of pickup loops: 1.05 gauss/mA

Mutual inductance to compensation coil: 2 mH

Heat Switch

Heater resistance: 10 kilohms

Heater current to drive switch normal: 1.50 mA

Normal state resistance of superconductor: 40 milli-ohms

Compensation Coil

Type of wire: T48B (See Note 1.)

Wire diameter including insulation: .11 mm (4.3 mils)

Number of turns: 32 (1 layer)

Coil length: .37 cm

Mean coil diameter: 1.51 cm

Coil resistance at room temperature: 15 ohms

Coil inductance: 22 micro-henry

Coaxial field at center: 26 gauss/amp

Carbon Resistance Thermometers

Fitting curve: $\frac{1}{T} = A + B\log_{10}R + C(\log_{10}R)^2$

where T is temperature in K

and R is resistance in kilohms

Least squares coefficients:

	R	A	B	C
Thermometer R_D	4-15	.103136	.190107	.040343
	15-30	-.172371	.616445	-.123500
	30-100	.306474	-.029666	.094490
Thermometer R_E	3-15	.107046	.196640	.039586
	15-27	-.065039	.470945	-.069328
	27-100	.293005	-.009388	.091776

Special temperatures:

T	R_D	R_E
300	.208	.199
77	.269	.253
4.2	4.16	3.89
1.6	100.0	90.1

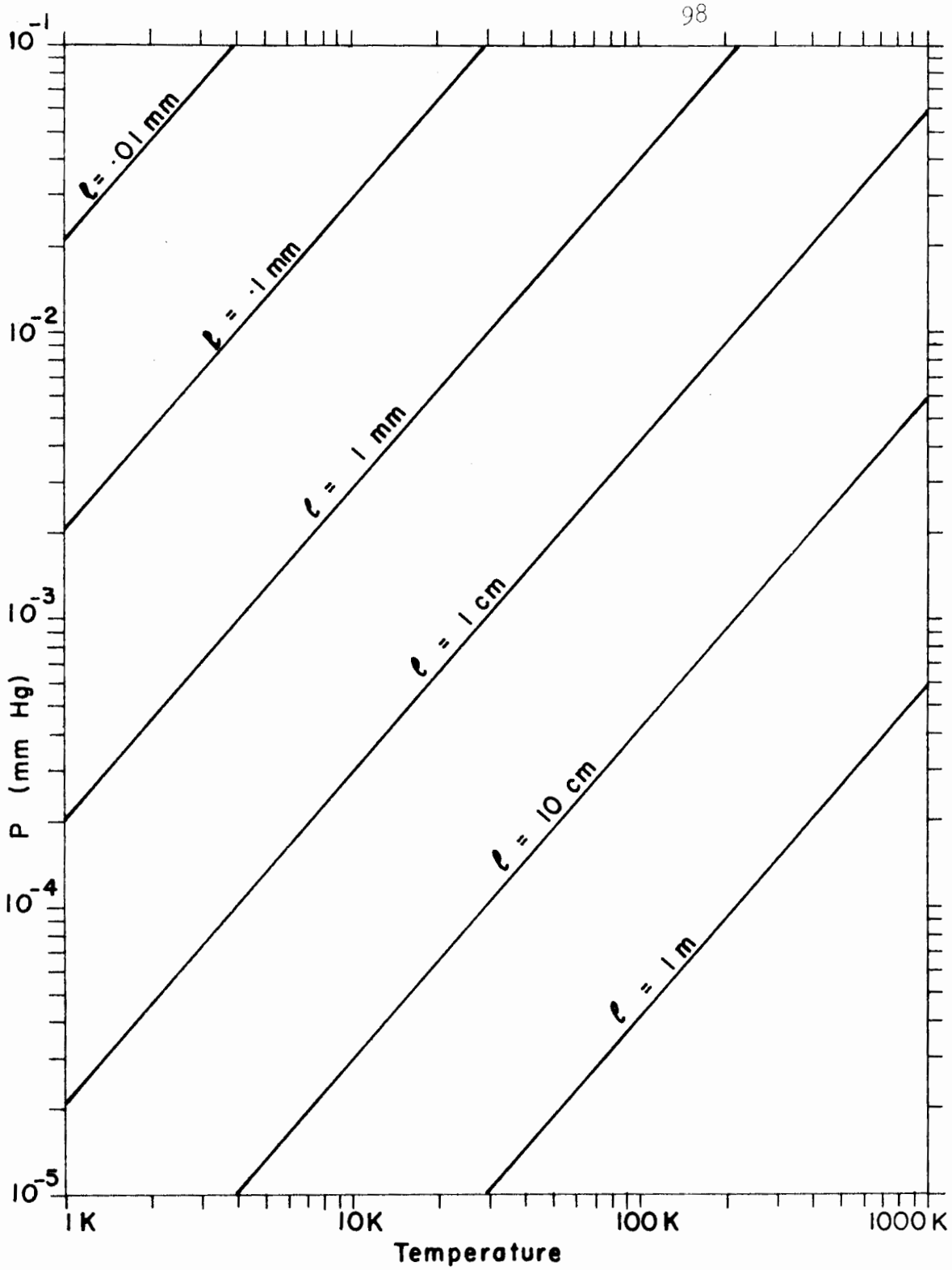

Figure 22: Mean free path, l, of He^4 gas. (Generated from $l = 2.16 \times 10^{-5} \frac{T}{P}^{1.15}$ cm from Reference 9.)

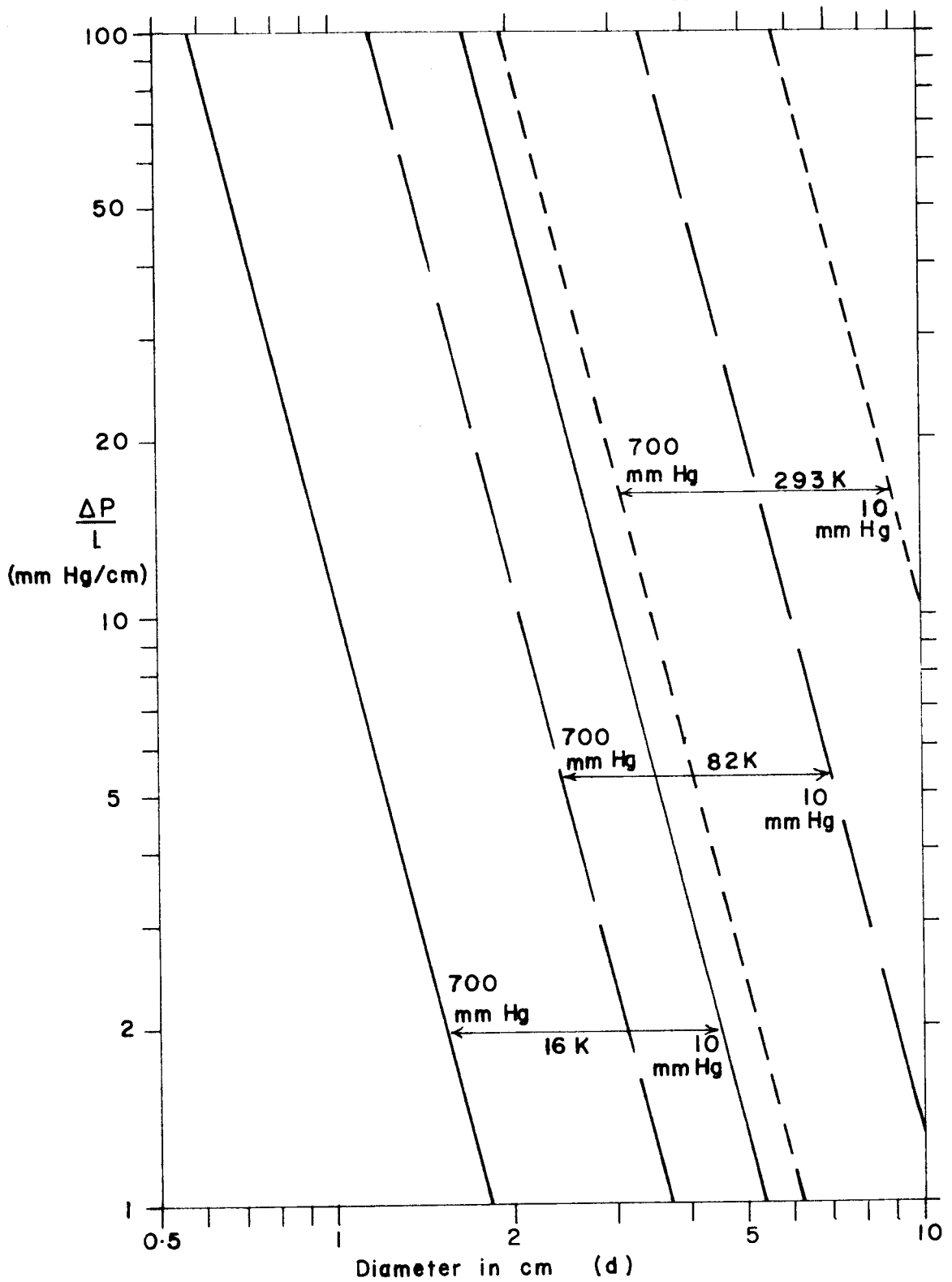

Figure 23: Pressure drop per unit length in circular tubing of inside diameter, d, carrying He^4 gas at a flow rate of .Ø1 moles/sec, or .2 std l/sec.

APPENDIX H

SECOND FLUX TRANSFORMER: The primary of this transformer would be a coil of as small a radius as possible, in which the sample would be situated. The secondary would be of as large a radius as the inside dimensions of the Sample Chamber will permit, situated coplanar with the present pickup loop.

In order to estimate the value of adding this second flux transformer, we will calculate the flux coupled to the pickup loop by such an arrangement. This quantity, which we will call ϕ_1', will be compared to ϕ_1, as given by Eq 30:

$$\phi_1 = 4\pi\chi H \frac{V}{2R} \qquad \text{Eq 30}$$

ϕ_1 is a measure of the coupling of the sample to the existing pickup loop.

There are several possible alternative choices of number and positioning of the additional coils. For simplicity, we will consider only the arrangement shown below.

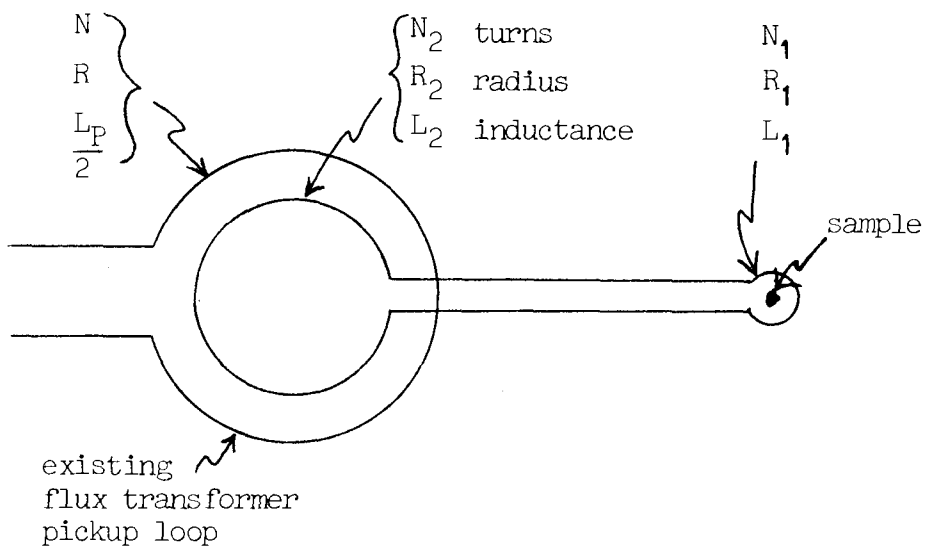

Figure 24

It is assumed that the transformer is provided with a switch of some sort so that the circuit may be broken in order to apply a field. We will also assume that the pickup loop of the existing flux transformer is some distance away from the sample so that direct coupling between them can be neglected in the calculation of ϕ_1'.

The coupling between the existing pickup loop and the secondary coil of the proposed flux transformer is determined by the mutual inductance of these two coils, M_{2P}. Therefore, by analogy to Eq 15,

$$\phi_1' = \frac{M_{2P}\, N_2}{L_1 + L_2}\, 4\pi\chi\, H\, \frac{V}{2R_1} \qquad \text{Eq 72}$$

where we have assumed that the sample is weakly coupled to the primary coil of the new transformer (cf Eq 28). ϕ'_1 is a measure of the coupling between the sample and the existing pickup loop via the second flux transformer.

The quantity of interest is given by the ratio

$$\frac{\phi_1'}{\phi_1} = \frac{M_{2P}\, N_2}{L_1 + L_2} \frac{R}{R_1} \qquad \text{Eq 73}$$

which is a measure of the signal enhancement obtained by the addition of the second transformer.

The inside dimensions of the Sample Chamber limit the radius of the secondary coil to less than .3 cm. In this range we can write

$$M_{2P} \simeq 2\pi^2 \times 10^{-9} \frac{R^2}{R_2} NN_2 \text{ henry} \qquad \text{Eq 74}$$

From Eq 3

$$L_1 \simeq 4\times10^{-8}\, R_1\, N_1^2 \text{ henry} \qquad \text{Eq 75}$$

$$L_2 \simeq 4\times10^{-8}\, R_2\, N^2 \text{ henry} \qquad \text{Eq 76}$$

where R, R_1, and R_2 are expressed in cm.

Maximizing the signal enhancement by adjusting N_1 and N_2 so that $L_1 = L_2$, we can now write

$$\phi_1' \simeq \frac{\pi^2 N R^3}{40 R_1 R_2^2} \qquad \text{Eq 77}$$

With existing values of N and R, and feasible values of R_1 and R_2, this ratio can easily reach 30.

Such a modification has the advantage of being relatively easy to implement besides the fact that an experimental run could still continue, albeit at reduced sensitivity, if the second flux transformer should fail to operate at any time.

The drawback of adding a second tranformer is the diamagnetism of the flux transformer itself; it would tend to exclude any imposed field from the region of the sample. This could be averted either by winding the second transformer astatically, or by fitting it with a heat switch so as to drive a section of the loop into the normal state for the purpose of applying a field. The former approach has the disadvantage of imposing a limitation upon the turns ratio of the transformer, thereby detracting from the degree of signal enhancement otherwise possible. The latter technique involves bringing the flux transformer in close contact with an external circuit, i.e. the heat switch control, with all of the noise problems inherent in so doing.

NOTES

1. The superconducting wire used for the heat switch, field coil, and compensation coil was Formvar insulated, copper-clad, type T48B wire obtained from the Supercon Division of the National Research Corporation, 9 Erie Drive, Natich, Massachusetts, 01762, U.S.A.

2. Niobium wire was obtained from the California Fine Wire Company, Grover City, California. All niobium wire used was .003 inch in diameter and insulated with H-Formvar.

3. Epoxies mentioned in the text were Stycast 2850FT with 24LV catalyst, and Stycast 1266, both manufactured by Emerson and Cuming Inc., Canton, Massachusetts, 02021, U.S.A.

REFERENCES

1. H.E. Barz, A.S. Cooper, E. Corenzwit, M. Marezio, B.T. Matthias, & P.H. Schmidt, Science, vol. 175, p884, 1972.

2. C. Berthier, D. Jerome, P. Molinie, & J. Rouxel, Solid State Comm., vol. 19, p131, 1976.

3. R.J. Birgeneau, J. Skalyo, & G. Shirane, Phys. Rev. B, vol. 3, p1736, 1971.

4. N. Boccara, J.P. Carton, & G. Sarma, Phys. Lett. A, vol. 49, p165, 1974.

5. L.N. Bulaevskii, Zh. Eksp. Teor. Fiz., vol. 64, p2241, 1973; (Sov. Phys. - JETP, vol. 37, p1133, 1973).

6. L.N. Bulaevskii, Zh. Eksp. Teor. Fiz., vol. 65, p1278, 1973; (Sov. Phys. - JETP, vol. 38, p634, 1974).

7. B.S. Chandrasekhar, Appl. Phys. Lett., vol. 1, p7, 1962; A.M. Clogston, Phys. Rev. Lett., vol. 9, p266, 1962.

8. L.E. Conroy & K.R. Pisharody, J. Solid State Chem., vol. 4, p345, 1972.

9. R.R. Conte, "Elements de Cryogenie", Masson & Cie., Paris, pp15-24, 1970.

10. S.D. Conte, "Elementary Numerical Analysis", McGraw-Hill, Toronto, p164, 1965.

11. R.J. Corrucini, Advances in Cryogenic Engineering, vol. 3, p353, 1957.

12. P. de Trey, S. Gygax, & J.-P. Jan, J. Low Temp. Phys., vol. 11, p421, 1973.

13. R.E. Dickerson, H.B. Gray, & G.P. Haight, Jr., "Chemical Principles", W.A. Benjamin, Inc., New York, 1970.

14. F.J. DiSalvo, "Proc. 13th Intnl. Conf. Low Temp. Phys.", Timmerhaus, O'Sullivan, & Hammel eds., vol. 3, p417, Plenum, New York, 1974.

15. F.J. DiSalvo, B.G. Bagley, J.M. Voorhoeve, & J.V. Waszczak, J. Phys. Chem. Solids, vol. 34, p1357, 1973.

16. F.J. DiSalvo, R. Schwall, T.H. Geballe, F.R. Gamble, & J.H. Osiecki, Phys. Rev. Lett., vol. 27, p310, 1971.

17. L. Dobrosavljevic, Phys. Stat. Sol. B, vol. 55, p773, 1973.

18. C.B. Duke, "Tunneling in Solids", Academic Press, 1969.

19. Feynman, Leighton, and Sands, "Lectures on Physics", vol. 3, Addison-Wesley, Toronto, 1966.

20. S. Foner, E.J. McNiff, Jr., A.H. Thompson, F.R. Gamble, T.H. Geballe, & F.J. DiSalvo, Bull. Am. Phys. Soc., vol. 17, p289, 1972.

21. P. Fulde & R.A. Ferrell, Phys. Rev. A, vol. 135, p550, 1964.

22. F.R. Gamble, F.J. DiSalvo, R.A. Klemm, & T.H. Geballe, Science, vol. 168, p568, 1970.

23. F.R. Gamble, J.H. Osiecki, M. Cais, R. Pisharody, F.J. DiSalvo, & T.H. Geballe, Science, vol. 174, p493, 1971.

24. F.R. Gamble, J.H. Osiecki, & F.J. DiSalvo, J. Chem. Phys., vol. 55, p3525, 1971.

25. T.H. Geballe, A. Menth, F.J. DiSalvo, & F.R. Gamble, Phys. Rev. Lett., vol. 27, p314, 1971.

26. R.R. Gerhardts, Phys. Rev. B, vol. 9, p2945, 1974.

27. Giffard, Webb, & Wheatley, J. Low-Temp. Phys., vol. 6, p533, 1972.

28. E. Godratt, A.J. Greenfield, & Y. Schlesinger, Cryogenics, vol. 17, p81, 1977.

29. B. Goodman (editor), "The Radio Amateur's Handbook", 42nd Edition, American Radio Relay League, Newington, Conn., U.S.A., 1965.

30. Hoare, Jackson, & Kurti, "Experimental Cryophysics", Butterworth & Co., London, 1961.

31. B. Horowitz & A. Birnboin, Solid State Comm., vol. 19, p91, 1976.

32. F. Hulliger, Structure and Bonding, vol. 4, p83, 1968.

33. J.D. Jackson, "Classical Electrodynamics", Wiley, New York, 1962.

34. F. Jellinek, J. Less-Common Metals, vol. 4, p9, 1962.

35. F. Jellinek, Arkiv Kemi, vol. 20, p447, 1963.

36. E.I. Kats, Zh. Eksp. Teor. Fiz., vol. 56, p1675, 1969; vol. 58, p1471, 1970, (Sov. Phys. - JETP, vol. 29, p897, 1969; vol. 31, p787, 1970).

37. C. Kittel, "Introduction to Solid State Physics", Wiley, Toronto, 1971.

38. R.A. Klemm, J. Low Temp. Phys. vol. 16, p381, 1974.

39. R.A. Klemm, M.R. Beasley, & A. Luther, Phys. Rev. B, vol. 8, p5072, 1973.

40. R.A. Klemm, M.R. Beasley, & A. Luther, J. Low Temp. Phys., vol. 16, p607, 1974.

41. R.A. Klemm, A. Luther, & M.R. Beasley, Phys. Rev. B, vol. 12, p877, 1975.

42. L.D. Landau & E.M. Lifshitz, "Fluid Mechanics", Pergamon Press, London and Paris, 1959.

43. A.I. Larkin & Yu. N. Ovchinnikov, Zh. Eksp. Teor. Fiz., vol. 47, p1136, 1964; (Sov. Phys. - JETP, vol. 20, p762, 1965).

44. W.E. Lawrence & S. Doniach, "Proc. 12th Intnl. Conf. Low Temp. Phys.", Academic Press, New York and London, p361, 1971.

45. O.V. Lounasmaa, "Experimental Principles and Methods Below 1K", Academic Press, London and New York, 1974.

46. A. Luther, M.R. Beasley, & R.A. Klemm, Nobel Symp., vol. 24, p149, 1973.

47. L.F. Mattheiss, Phys. Rev. B, vol. 8, p3719, 1973.

48. R.C. Morris & R.V. Coleman, Phys. Rev. B, vol. 7, p991, 1973.

49. W.L. Pillinger, P.S. Jastram, & J.G. Daunt, The Review of Scientific Instruments, vol. 29, p159, 1958.

50. D.E. Prober, "Magnetic Properties of Superconducting Layered Compounds", Technical Report No. 10, Division of Engineering and Applied Physics, Harvard University, Cambridge, Massachusetts, U.S.A., 1975.

51. D.E. Prober, M.R. Beasley, & R.E. Schwall, "Proc. 13th Intnl. Conf. Low Temp. Phys.", Timmerhaus, O'Sullivan, & Hammel eds., vol. 3, p428, Plenum Press, New York, 1974.

52. E.M. Purcell, "Electricity and Magnetism", McGraw-Hill, Toronto, 1965.

53. E. Revolinski, G.A. Spiering, & D.J. Beernsten, J. Phys. Chem. Solids, vol. 26, p1029, 1965.

54. B.W. Roberts, J. Phys. Chem. Ref. Data, vol. 5, p581, 1976.

55. A.C. Rose-Innes, "Low Temperature Techniques", Van Nostrand, Princeton, New Jersey, 1964.

56. H.M. Rosenberg, "Low Temperature Solid State Physics", Clarendon Press, Oxford, 1963.

57. J.W. Stout, & L. Guttman, Phys. Rev., vol. 88, p703, 1952.

58. M. Strongin, A. Paskin, D.G. Schweitzer, O.F. Kammerer, & P.P. Craig, Phys. Rev. Lett., vol. 12, p442, 1964.

59. A.H. Thompson, F.R. Gamble, & R.F. Koehler, Jr., Phys. Rev. B, vol. 5, p2811, 1972.

60. A.H. Thompson, F.R. Gamble, & J.F. Revelli, Solid State Comm., vol. 9, p981, 1971.

61. J.P. Tidman, O. Singh, A.E. Curzon, & R.F. Frindt, Phil. Mag., vol. 30, p1191, 1974.

62. T. Tsuzuki, J. Low Temp. Phys., vol. 9, p525, 1972.

63. M.H. van Maaren & H.B. Harland, Phys. Lett., vol. 29A, p571, 1969.

64. J.M. Voorhoeve & M. Robbins, J. Solid St. Chem., vol. 1, p134, 1970.

65. W.H. Warren Jr., & W.G. Bader, The Review of Scientific Instruments, vol. 40, p180, 1969.

66. N.R. Werthamer in "Superconductivity", edited by R.D. Parks, Marcel Dekker, Inc., New York, 1969.

67. J.C. Wheatley, The Review of Scientific Instruments, vol. 35, p765, 1964.

68. G.K. White, "Experimental Techniques in Low-Temperature Physics", Clarendon Press, Oxford, 1959.

69. J. Wilks, "Properties of Liquid and Solid Helium", Clarendon Press, Oxford, 1967.

70. J.A. Wilson & A.D. Yoffe, Adv. Phys., vol. 18, p193, 1969.

71. J.A. Woollam, R.B. Somoano, & P. O'Connor, Phys. Rev. Lett., vol. 32, p712, 1974.

72. J.E. Zimmerman, & W.H. Campbell, Geophysics, vol. 40, p269, 1975.

73. J.E. Zimmerman, J. Appl. Phys., vol. 48, p702, 1977.

74. Supplement au Journal de Physique, Colloque C-4, 1976.

75. "The 1958 He^4 Scale of Temperatures", U.S. Department of Commerce, National Bureau of Standards.

76. "Handbook of Chemistry and Physics", 54th Edition, Chemical Rubber Publishing Company, Cleveland, Ohio, 1973.